Monthly Notices
of the
ROYAL ASTRONOMICAL SOCIETY

MNRAS **445,** 1820–1835 (2014) doi:10.1093/mnras/stu1829

Subhalo statistics of galactic haloes: beyond the resolution limit

Marius Cautun,[1,2]★ Wojciech A. Hellwing,[1,3] Rien van de Weygaert,[2]
Carlos S. Frenk,[1] Bernard J. T. Jones[2] and Till Sawala[1]

[1]*Department of Physics, Institute for Computational Cosmology, University of Durham, South Road Durham DH1 3LE, UK*
[2]*Kapteyn Astronomical Institute, University of Groningen, PO Box 800, NL-9747 AV Groningen, the Netherlands*
[3]*Interdisciplinary Centre for Mathematical and Computational Modelling, University of Warsaw, ul. Pawińskiego 5a, PL-02-106, Warsaw, Poland*

Accepted 2014 September 4. Received 2014 July 10; in original form 2014 March 25

ABSTRACT

We study the substructure population of Milky Way (MW)-mass haloes in the Λ cold dark matter (ΛCDM) cosmology using a novel procedure to extrapolate subhalo number statistics beyond the resolution limit of *N*-body simulations. The technique recovers the mean and the variance of the subhalo abundance, but not its spatial distribution. It extends the dynamic range over which precise statistical predictions can be made by the equivalent of performing a simulation with 50 times higher resolution, at no additional computational cost. We apply this technique to MW-mass haloes, but it can easily be applied to haloes of any mass. We find up to 20 per cent more substructures in MW-mass haloes than found in previous studies. Our analysis lowers the mass of the MW halo required to accommodate the observation that the MW has only three satellites with a maximum circular velocity $V_{\rm max} \geq 30\,{\rm km\,s^{-1}}$ in the ΛCDM cosmology. The probability of having a subhalo population similar to that in the MW is 20 per cent for a virial mass, $M_{200} = 1 \times 10^{12}\,{\rm M_\odot}$ and practically zero for haloes more massive than $M_{200} = 2 \times 10^{12}\,{\rm M_\odot}$.

Key words: Galaxy: abundances – Galaxy: halo – cosmology: theory – dark matter.

1 INTRODUCTION

The standard 'Λ cold dark matter' (ΛCDM) cosmological model has been found to give a good description of structure formation and evolution on scales $\gtrsim$10 Mpc. This has been confirmed by multiple observational probes: the cosmic microwave background temperature anisotropies (eg. Komatsu et al. 2011; Planck Collaboration 2013), large-scale galaxy clustering (eg. Cole et al. 2005) and the expansion history of the Universe (e.g. Clocchiatti et al. 2006; Guy et al. 2010). On smaller scales, the ΛCDM predictions are more difficult to extract and test due both to the non-linear evolution of the matter distribution and the complex hydrodynamical processes that drive galaxy formation and evolution. Nonetheless, it is this regime that is especially interesting and important for cosmology as it can potentially constrain the nature of the dark matter (DM) and the baryonic processes involved in galaxy formation. Our own Milky Way (MW) galaxy and its satellites play a crucial role in this due to their proximity which enables in-depth studies.

Several of the apparent points of tension between observations and ΛCDM predictions are seen in the properties of the MW and its satellites. The phrase 'missing satellites problem' is often incorrectly used to refer to the apparent discrepancy between the large number of DM subhaloes in *N*-body simulations, first highlighted by Moore et al. (1998), and the handful of satellites detected around the MW. In fact, this 'problem' simply reflects the well-known fact that most of the DM subhaloes never manage to acquire a visible galaxy because of inevitable physical processes, such as reionization and the injection of supernova energy, that are an intrinsic part of galaxy formation (Bullock, Kravtsov & Weinberg 2000; Benson et al. 2002b; Somerville 2002).

A more significant 'satellite problem', recognized as such already by Klypin et al. (1999) and Moore et al. (1999), is the apparent discrepancy between the distribution of the maximum circular velocities of the most massive subhaloes in ΛCDM simulations and the inferred values for the MW's satellites. Various arguments based on the kinematics of the nine bright 'classical' dwarf spheroidal satellites of the MW suggest that their subhaloes have maximum circular velocities $V_{\rm max} \lesssim 30\,{\rm km\,s^{-1}}$ (Peñarrubia, McConnachie & Navarro 2008; Strigari et al. 2008; Łokas 2009; Walker et al. 2009; Strigari, Frenk & White 2010; Wolf et al. 2010; Boylan-Kolchin, Bullock & Kaplinghat 2011, 2012). These are lower than the values for the most massive subhaloes in simulations of galactic haloes such as the high-resolution simulations of the Aquarius project (Springel et al. 2008). Specifically, Boylan-Kolchin et al. (2011, 2012) brought attention to the observation that these simulations typically produce around eight subhaloes with $V_{\rm max} > 30\,{\rm km\,s^{-1}}$, whereas in the MW only the two Magellanic Clouds and the Sagittarius dwarf are thought to reside in subhaloes with such high circular velocities. This raises the possibility that

★ E-mail: marius.cautun@gmail.com

there could be several massive substructures in the MW without a luminous galaxy in them. The high mass (HM) of these subhaloes, however, makes this rather unlikely given that less massive subhaloes do have satellite galaxies associated with them.

A possible solution to this so-called 'too-big-to-fail' problem was proposed by (Wang et al. 2012, hereafter Wang12) who showed that the presence of only three massive satellites in our galaxy is consistent with ΛCDM predictions provided the mass of the MW dark halo is $\sim 1 \times 10^{12}\,\mathrm{M}_\odot$, around half the average mass of the haloes in the Aquarius simulations analysed by Boylan-Kolchin et al. (2011, 2012, see also Purcell & Zentner 2012; Vera-Ciro et al. 2013). Wang12 used the invariance of the scaled subhalo velocity function (e.g. Moore et al. 1999; Kravtsov et al. 2004; Zheng et al. 2005; Springel et al. 2008; Weinberg et al. 2008) to extend the subhalo number statistics derived from *N*-body simulations of large cosmological volumes to galactic haloes. This allowed them to compute, as a function of halo mass, the probability of having a satellite population similar to that of the MW. The outcome of this calculation favours an MW halo mass at the lower end of the range spanned by recent estimates (Wilkinson & Evans 1999; Sakamoto, Chiba & Beers 2003; Battaglia et al. 2005; Dehnen, McLaughlin & Sachania 2006; Smith et al. 2007; Li & White 2008; Xue et al. 2008; Gnedin et al. 2010; Guo et al. 2010; Watkins, Evans & An 2010; Busha et al. 2011a; Piffl et al. 2014).

Characterizing how typical the MW satellites are in ΛCDM requires large samples of simulated MW-mass haloes. Simulations of large cosmological volumes provide these but, so far, only at relatively low resolution, probing only the most massive subhaloes ($\lesssim$10 substructures per MW halo; Boylan-Kolchin et al. 2009; Klypin, Trujillo-Gomez & Primack 2011). By contrast, high-resolution 'zoom' simulations of individual MW-like haloes resolve substructures down to much lower masses, but because of their large computational cost, only a few examples have been simulated so far and these are not guaranteed to be characteristic of an MW-like halo population (Diemand et al. 2008; Springel et al. 2008; Stadel et al. 2009). Some of the alleged points of tension between observations and models rely on such high-resolution, but limited-sample studies, and one cannot exclude the possibility that these discrepancies reflect the inherent cosmic variance of small-volume studies.

In this work, we introduce a new method for extending subhalo statistics beyond the resolution limit available to cosmological simulations. This allows us to investigate the statistical properties of the subhalo population of a representative sample of MW-mass haloes down to substructures with $V_{\rm max} \gtrsim 15\,\mathrm{km\,s^{-1}}$, which represents a threefold increase in the $V_{\rm max}$ range compared to related previous studies (e.g. Boylan-Kolchin et al. 2010, hereafter BK10; Wang12). Making use of our extrapolation method, we can check previous subhalo count results, such as those of Wang12, over a larger dynamical range in subhalo mass. In particular, we analyse the dependence of the mean subhalo count on halo mass and revisit the probability of finding a satellite population similar to that in the MW.

Our extrapolation method should not be confused with semi-analytical models for DM substructure (e.g. Benson et al. 2002a, and the later refinements of Zentner et al. 2005; Jiang & van den Bosch 2014). Our method statistically generates the correct subhalo abundance from the partial information available in a simulation of limited resolution. In contrast, semi-analytical models are based on halo merger trees and on the treatment of the various physical processes that affect the evolution of subhaloes. While such models are significantly faster than numerical simulations, they are limited because of their approximate treatment of relevant physical processes.

Table 1. The cosmological and numerical parameters of the three *N*-body simulations used in this study.

Parameter	MS	MS-II	*WMAP*7
Box size (h^{-1} Mpc)	500	100	70.4
Particle number	2160^3	2160^3	1620^3
Particle mass ($10^6\,h^{-1}\,\mathrm{M}_\odot$)	860	6.89	6.2
$\Omega_{\rm m}$	0.25	0.25	0.272
Ω_Λ	0.75	0.75	0.728
σ_8	0.9	0.9	0.81
h	0.73	0.73	0.704
$n_{\rm s}$	1	1	0.968
Force softening (h^{-1} kpc)	5	1	1

In Section 2, we describe the simulations we use and the halo/subhalo identification algorithm. In Section 3, we introduce the scaling method for extending the subhalo statistics to masses that are unresolved in the simulations. In Sections 4 and 5, we investigate the subhalo population of MW-like haloes. Given that we find significantly more subhaloes than previous studies, in Section 6 we revisit the constraints on the MW halo mass required to avoid the too-big-to-fail problem. In Section 7, we study how typical the Aquarius haloes are compared to a representative sample of MW-like hosts. We end with a brief summary in Section 8.

2 DATA ANALYSIS

In this study, we analyse the two high-resolution Millennium simulations[1] (MS; Springel et al. 2005 and MS-II; Boylan-Kolchin et al. 2009). Both are DM-only simulations and make use of 2160^3 particles to resolve structure formation in the *Wilkinson Microwave Anisotropy Probe* (*WMAP*)-1 cosmogony (Spergel et al. 2003). The MS models cosmic evolution in a periodic volume of length $500\,h^{-1}$ Mpc with a mass per particle of $m_{\rm p} = 8.6 \times 10^8\,h^{-1}\,\mathrm{M}_\odot$. The large volume of the simulation makes it ideal for the study of substructures in cluster and group sized objects, but it is of limited use for MW-sized haloes which are resolved with only $\sim 10^3$ particles. The MS-II resolves structure formation in a much smaller box of $100\,h^{-1}$ Mpc on a side with a particle mass of $m_{\rm p} = 6.89 \times 10^6\,h^{-1}\,\mathrm{M}_\odot$. The lower mass per DM particle makes it suitable for studying MW-like haloes that are resolved with around 10^5 particles, but its smaller volume precludes a systematic study of higher mass objects. The parameters used in the two simulations are given in Table 1.

The difference in the resolution of the two simulations, with equal mass haloes being resolved with 125 times more particles in MS-II than in MS, makes it possible to carry out convergence tests and other tests of the numerical effects on the subhalo population.

We also analyse a 1620^3 particle *N*-body simulation of a volume $70.4\,h^{-1}$ Mpc on a side in the *WMAP*-7 cosmology (Komatsu et al. 2011). This has a similar particle mass to the MS-II, $m_{\rm p} = 6.2 \times 10^6\,h^{-1}\,\mathrm{M}_\odot$, but only a third of the MS-II volume. We refer to this additional simulation as *WMAP*7 and use it to investigate the differences between the predictions of *WMAP*-1 and *WMAP*-7 ΛCDM universes.

[1] Data from the Millennium/Millennium-II simulation is available on a relational data base accessible from http://galaxy-catalogue.dur.ac.uk:8080/Millennium.

For comparative purposes, we also make use of the Aquarius Project data (Springel et al. 2008), a set of MW-mass DM haloes simulated at very high resolution in the *WMAP*-1 cosmology. The six haloes, denoted Aq.-A through Aq.-F, were selected from the MS-II and resimulated at increasingly higher resolution. Here, we make use of the 'level-2' haloes that have a particle mass of $\sim 10^4\, h^{-1}\, \mathrm{M}_\odot$ and gravitational softening of $48\, \mathrm{h}^{-1}\mathrm{pc}$.

2.1 Halo finder

We identify haloes and subhaloes using the ROCKSTAR (Robust Overdensity Calculation using K-Space Topologically Adaptive Refinement) phase-space halo finder (Behroozi, Wechsler & Wu 2013). ROCKSTAR starts by selecting potential haloes as Friends-of-Friends (FOF; Davis et al. 1985) groups in position space using a large linking length ($b = 0.28$ the mean interparticle separation). This first step is restricted to position space to optimize the use of computational resources, while subsequent steps employ the full 6D phase space. Each FOF group from the first step is used to create a hierarchy of FOF phase-space subgroups by progressively reducing the linking length. The phase-space subgroups are selected using an adaptive phase-space linking length such that each successive subgroup has 70 per cent of the parent's particles. ROCKSTAR uses the resulting subgroups to identify potential halo and subhalo centres and assigns particles to them based on their phase-space proximity. Once all particles are assigned to haloes and subhaloes, an unbinding procedure is applied to retain only gravitationally bound particles. The final halo centres are computed from a small region around the phase-space density maximum of each object.

The outer boundary of the haloes is defined as the distance at which the enclosed overdensity decreases below $\Delta = 200$ times the critical density, ρ_c. Therefore, the halo mass, M_{200}, and radius, R_{200}, correspond to a spherical overdensity of $200\rho_\mathrm{c}$. Using this definition for the main halo boundary, we identify all subhaloes within distance R_{200} from the host halo centre as the satellite population. A typical MW-mass halo with $M_{200} = 10^{12}\, \mathrm{M}_\odot$ has $R_{200} \approx 200\, \mathrm{kpc}$ which is smaller than the maximum distance commonly used to identify dwarf galaxies in the MW; for example Leo I is considered an MW satellite but it is located $\sim$250 kpc from our galaxy (Karachentsev et al. 2004). We therefore apply a second criterion and identify as subhaloes all the objects within R_{100} from the host centre. The distance R_{100} is the radius within which the enclosed overdensity decreases to $100\rho_\mathrm{c}$ and is typically $\sim$1.3 times larger than R_{200}. We denote this second group of subhaloes as R_{100} substructures.

3 EXTRAPOLATING SUBHALO STATISTICS BEYOND THE RESOLUTION LIMIT

There are two challenges when studying the satellite population in numerical simulations: identifying the subhaloes and correctly determining their internal structure and orbits. Identifying an object made of a few tens to hundreds of particles against the background of a much bigger halo is not trivial and most configuration-space halo finders have difficulties finding subhaloes of fewer than 50 particles as well as larger subhaloes located close to the centre of the host. While phase-space finders (which includes ROCKSTAR) perform somewhat better, they still have problems recovering the correct properties of substructures containing tens of particles (for additional details see Knebe et al. 2011). Even when a halo finder identifies substructures, their properties can be affected by numerical resolution. Before accretion, the main effect of resolution is on the inner structure of the subhalo. After accretion, poor resolution can affect the orbit and tidal stripping of the subhalo. While these effects are subdominant for subhaloes resolved with a large number of particles, they are very important for subhaloes resolved with around 100 particles or less.

Resolution effects play an important role in establishing the extent to which a given simulation can correctly probe the subhalo population. In what follows, we introduce a scaling method that allows us to extrapolate the subhalo statistics beyond the resolution limit of a simulation. Applying this algorithm to an *N*-body simulation involves two main steps.

(I) Determining the range over which numerical effects influence the subhalo count. In general, a simulation correctly follows all substructures above a certain particle number, but resolves only a fraction of smaller subhaloes. This results in missing substructures and a systematic underestimate of the subhalo number count.

(II) Adding the missing subhaloes in the range where only a partial subhalo population is found. This procedure recovers the mean and scatter of the subhalo abundance down to much lower subhalo masses than are resolved in the simulation.

In the remainder of this section, we describe our method in more detail and demonstrate how to use it to infer the true subhalo abundance in the two MS.

3.1 Step I: quantifying the resolution effects

Since the CDM linear power spectrum of fluctuations has power on all scales down to an Earth mass, $\sim 10^{-6}\, h^{-1}\, \mathrm{M}_\odot$, increasing the resolution of a simulation results not only in a better determination of the internal structure of HM satellites, but also in the generation of new, and previously not resolved, lower mass subhaloes. To study finite resolution effects, we consider the abundance of subhaloes as a function of the substructure to host size ratio. The mass of a subhalo is not a well-defined quantity because it depends on the definition of the subhalo's boundary and on the gravitational unbinding procedure. A more robust way to characterize subhalo size is through the maximum circular velocity, V_max. This is determined by the inner structure of the object and is therefore relatively insensitive to the identification algorithm or the definition of boundary (for details see Onions et al. 2012). Furthermore, using V_max to characterize the size of satellites lends itself to a closer comparison with observations that typically probe only the inner part of a halo where the galaxy resides. Thus, rather than the mass ratio, we will consider the ratio of V_max to the host virial velocity, V_{200}, defined as

$$V_{200} = \sqrt{\frac{G M_{200}}{R_{200}}}, \tag{1}$$

with G the gravitational constant.

We parametrize the substructure to host halo velocity ratio as

$$\nu = \frac{V_\mathrm{max}}{V_{200}}\,, \tag{2}$$

where V_max refers to the subhalo and V_{200} to the host halo. We define $\overline{N}(>\nu)$ as the average number of subhaloes per host with velocity ratio exceeding ν. Given a sample of haloes within a chosen mass or V_{200} range, the mean subhalo count is given by

$$\overline{N}(>\nu) = \frac{1}{n_\mathrm{hosts}} \sum_{i=1}^{n_\mathrm{hosts}} N_i(>\nu)\,, \tag{3}$$

where $n_{\rm hosts}$ denotes the numbers of haloes in the sample and $N_i(>\nu)$ gives the number of subhaloes with velocity ratio exceeding ν in halo i. The derivative of this quantity,

$$\overline{N}(\nu) = \frac{{\rm d}\overline{N}(>\nu)}{{\rm d}\nu}, \tag{4}$$

gives the mean number of subhaloes per host with velocity ratio in the range ν to $\nu + {\rm d}\nu$ per ${\rm d}\nu$ interval.

Lack of numerical resolution will result in fewer than expected substructures in an N-body simulation. For example, subhaloes traced by $\lesssim$100 particles tend to have artificially low maximum circular velocities because of the gravitational softening (Springel et al. 2008). The resulting lower concentration makes them vulnerable to premature tidal disruption after they fall into the host halo. We quantify the effects resolution on the subhalo number counts by expressing

$$\overline{N}(\nu) = \widetilde{N}(\nu) f(\nu), \tag{5}$$

where $\widetilde{N}(\nu)$ is the true subhalo count at ν in the absence of resolution effects. The function $f(\nu)$ is the completeness function that describes the artificial loss of subhaloes due to limited numerical resolution. A value of $f(\nu) = 1$ means that the simulation has resolved all the substructures at ν while values of $f(\nu) < 1$ mean that only a partial population of subhaloes has been detected. Thus, quantifying this kind of resolution effect reduces to measuring the completeness function, $f(\nu)$, for a given simulation.

There is a wide range of factors that can influence the completeness function of cosmological simulations: gravitational softening length, integration timestep and other numerical parameters, to the halo finder and the code used to run the simulation. Exploring such a large parameter space to provide a general formula for $f(\nu)$ would be unfeasible, so instead we will show how to compute the function $f(\nu)$ for any given N-body simulation. Within the same simulation, the completeness function will likely depend on the mass of the host halo. We parametrize this dependence via the number of particles, $\mathcal{N}$, with which the host halo is resolved. Note that we use $\overline{N}$ to denote the mean subhalo count and $\mathcal{N}$ to denote the number of DM particles in the host halo.

To estimate the completeness function, we compare the substructure count between haloes in simulations with two different resolutions. The result is illustrated in Fig. 1 where we contrast the mean subhalo count of (0.6–1.2) $\times\ 10^{13}\,h^{-1}\,{\rm M}_\odot$ mass haloes that were resolved at low resolution in MS and at high resolution in the MS-II. To emphasize the difference we plot the ratio, $\overline{N}_{\rm MS}(\nu)/\overline{N}_{\rm MS\text{-}II}(\nu)$, between the subhalo count in the two simulations. Since $\sim 10^{13}\,h^{-1}\,{\rm M}_\odot$ mass haloes in the MS-II have over 10^6 particles, we expect $\overline{N}_{\rm MS\text{-}II}(\nu)$ to be unaffected by numerical effects for $\nu \gtrsim 0.15$ (for a detailed justification of this point see Appendix A1). This implies that for $\nu \gtrsim 0.15$, we have $\overline{N}_{\rm MS\text{-}II}(\nu) \approx \widetilde{N}(\nu)$ and so, according to equation (5), the ratio $\overline{N}_{\rm MS}(\nu)/\overline{N}_{\rm MS\text{-}II}(\nu)$ gives the completeness function of MS haloes.

Fig. 1 shows that the completeness function is flat and equal to 1 at values of $\nu > 0.4$, indicating that in that range the MS recovers the full population of substructures. At lower values of ν, the completeness function decreases from 1 to 0 reflecting the fact that only a partial population of subhaloes is found in that range in the MS. This is in agreement with the qualitative expectation discussed above. The transition in the MS completeness function from 1 to 0 is well approximated by a linear function of $\log \nu$, as

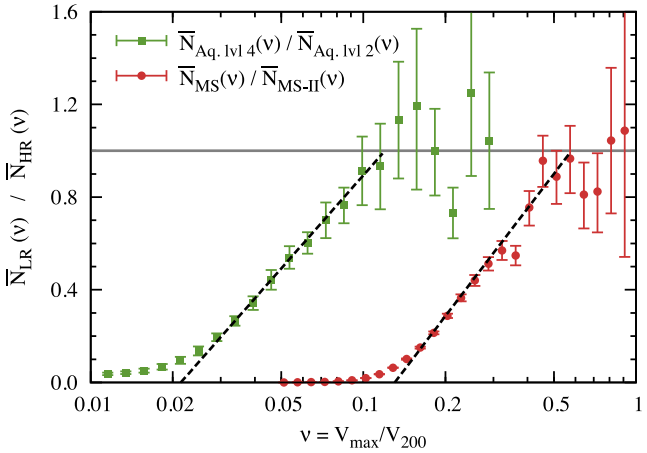

Figure 1. Comparison of the mean subhalo number, $\overline{N}(\nu)$, between equal mass haloes resolved at two different resolutions. The circles show haloes in the mass range (0.6–1.2) $\times\ 10^{13}\,h^{-1}\,{\rm M}_\odot$ that were resolved with (0.7–1.4) $\times\ 10^4$ particles in the MS and with 125 times more particles in the MS-II. The squares compare $\overline{N}(\nu)$ of the Aquarius haloes resolved with $\sim 10^7$ particles at 'level-4' and with $\sim$20 times more particles at 'level-2'. The dashed curve shows that the transition from 1 to 0 is well approximated by a linear function in $\ln \nu$. The error bars represent the 1σ uncertainty in the determination of the ratio between the two subhalo numbers.

shown by the dashed line in the figure. Therefore, we can write the completeness function as

$$f(\nu) = \begin{cases} 1 & \nu \geq \nu_0 \\ 1 + \alpha \ln\left(\frac{\nu}{\nu_0}\right) & \nu_* < \nu < \nu_0 \\ 0 & \nu < \nu_*, \end{cases} \tag{6}$$

where α and ν_0 are two free parameters (and ln denotes the natural logarithm). The α parameter gives the slope of the transition from 1 to 0, while ν_0 gives the smallest value of ν for which the simulation identifies all the substructures. The symbol, $\nu_* = \nu_0 {\rm e}^{-1/\alpha}$, denotes the point below which no more subhaloes are detected. This expression gives a very good match to the completeness function as long as $f(\nu) \gtrsim 0.2$, as can be seen in the figure.

In Appendix A2, we show that the two parameter fit in equation (6) gives a very good description of the completeness function not only for the MS and Aquarius haloes, but also for the MS-II and *WMAP*7 simulations. Furthermore, we have checked that the same holds true when using different halo finders.

Thus, computing the completeness function of any given simulation reduces to finding the ν_0 and α parameters introduced in equation (6). We propose two different methods to calculate these parameters. These procedures are described in detail in Appendix A and can be summarized as follows.

(a) *Method A* is the standard procedure of comparing haloes of equal mass in simulations of different resolution. We used this method to compute $f(\nu)$ for the MS by comparing with the higher resolution MS-II data. While this method is simple to implement, it has the drawback that it requires an additional simulation with $\sim$100 times higher mass resolution than the simulation of interest. Therefore, we can use method A for MS, but not for the MS-II and *WMAP*7 since we do not have access to even higher resolution simulations. We introduce method A merely to show that our second technique, method B, gives reliable results.

(b) *Method B* compares the subhalo population in LM and HM haloes in the same simulation. The procedure is based on the

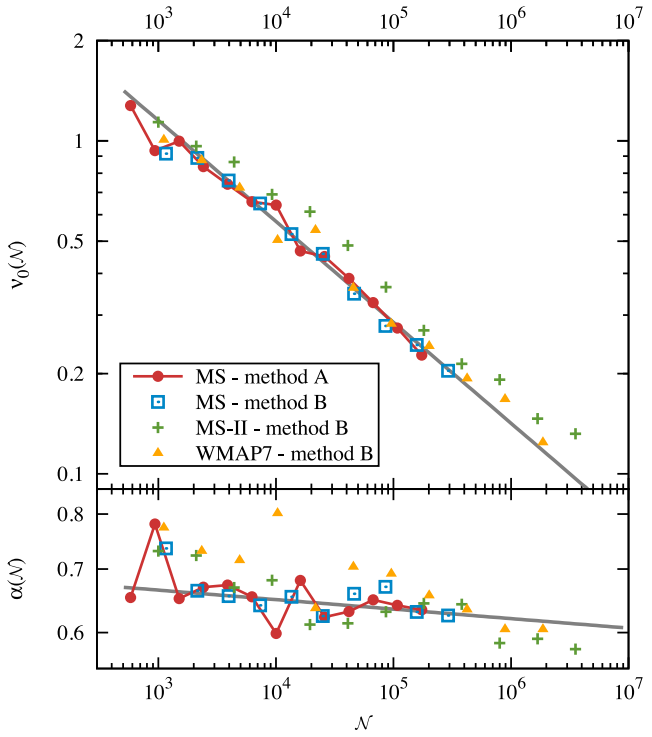

Figure 2. The dependence of the completeness function fit parameters, ν_0 (top panel), and α (lower panel), on the number of particles, $\mathcal{N}$, in the host halo. The fit parameters were determined using the two different methods, A and B, described in Appendix A. The solid grey line shows a power-law fit to the results of method A. The power-law fits to each of the simulations are given in Table 2.

assumption that the mean subhalo count is self-similar amongst host haloes of different masses (see Wang et al. 2012, and references therein). As we shall see in Section 5, this assumption is satisfied to a good approximation for DM substructures but the addition of baryons and feedback processes would break the self-similar behaviour so it is unclear if this procedure can be modified to work in realistic hydrodynamical simulations of galaxy formation. Compared to method A, method B does not require a higher resolution simulation. This represents a great advantage and allows us to compute the completeness function for the MS-II and *WMAP*7 simulations.

Using the two methods above, we estimate the completeness function for host haloes of different mass. We find that the two fitting parameters for $f(\nu)$ in equation (6) depend most strongly on the number of particles, $\mathcal{N}$, used to resolve the host halo. This relationship is illustrated in Fig. 2. The α and ν_0 parameters show a power-law dependence on $\mathcal{N}$:

$$\nu_0(\mathcal{N}) = \nu_0^0 \left(\frac{\mathcal{N}}{10^4}\right)^{n_{\nu_0}} \quad \text{and} \quad \alpha(\mathcal{N}) = \alpha^0 \left(\frac{\mathcal{N}}{10^4}\right)^{n_\alpha}. \tag{7}$$

The quantities, ν_0^0, n_{ν_0}, α^0 and n_α, are constants that depend on the numerical parameters of the simulation, but not on $\mathcal{N}$. The two expressions in equation (7) give a very good description of $\nu_0(\mathcal{N})$ and $\alpha(\mathcal{N})$. This is clearly shown in the figure by the grey line which gives a power-law fit to the results of method A applied to the MS (solid red line with circular symbols).[2] The power-law fits to α and ν_0 for the three simulations shown in Fig. 2 are given in Table 2. All the simulations show the same qualitative behaviour, though the exact values differ slightly. The quantity ν_0 varies as $\mathcal{N}^{-0.3}$, which is close to, but shallower than the $\mathcal{N}^{-1/3}$ dependence that a naive kinematic analysis would suggest. The parameter α varies only slightly, as $\mathcal{N}^{-0.02}$.

Table 2. The values of the variables ν_0^0, n_{ν_0}, α^0 and n_α given in equation (7). These quantities give the dependence of the fitting parameters of the completeness function, ν_0 and α, on the number of particles, $\mathcal{N}$, in the host halo. We give values for subhaloes within distance, R_{200}, and, R_{100}, from the host halo centre. The 1σ error in the fit for ν_0^0 and α^0 is 0.02, while that for n_{ν_0} and n_α is 0.01.

Method – simulation	ν_0^0	n_{ν_0}	α^0	n_α
R_{200} substructures				
Method A – MS	0.57	−0.30	0.65	−0.01
Method B – MS	0.57	−0.31	0.65	−0.01
Method B – MS-II	0.67	−0.29	0.67	−0.02
Method B – *WMAP*7	0.57	−0.29	0.72	−0.03
R_{100} substructures				
Method A – MS	0.55	−0.30	0.65	−0.02
Method B – MS	0.55	−0.31	0.65	−0.01
Method B – MS-II	0.67	−0.29	0.65	−0.03
Method B – *WMAP*7	0.56	−0.28	0.72	−0.04

Fig. 2 shows that the two methods, A and B, for estimating the completeness function give the same results. This is clearly seen when comparing the values of ν_0 and α for the MS simulation obtained using method A (solid red line) and method B (blue square symbols). Thus, $f(\nu)$ can be computed only using the information available in the simulation under study without the use of a higher resolution simulation, by following the method B procedure outlined in Appendix A2.

In addition, Fig. 2 shows that there are small differences between the completeness function of the three simulations studied here (see also Table 2). Therefore, when precise results are needed, it is necessary to estimate $f(\nu)$ separately for each simulation. Computing the completeness function of a given simulation can be done with minimal computational resources using method B.

The results presented up to now are for substructures within distance, R_{200}, of the host halo centre. We find that the fitting formula of equation (6) with very similar parameter values also describes well the completeness function for subhaloes within R_{100} of the host halo centre (see Table 2).

3.2 Step II: adding the missing subhaloes

As we have seen, the completeness function can be used to estimate the mean abundance of poorly resolved or unresolved subhaloes as a function of $V_{\rm max}$. However, in practice, it is necessary to know not only the mean value of $\overline{N}(>\nu)$, but also its dispersion $\sigma(>\nu)$ across the halo population, which characterizes the halo-to-halo variation.

Given a completeness function, $f(\nu)$, lack of resolution implies that a sample of $n_{\rm hosts}$ haloes are missing a fraction, $1 - f(\nu)$, of their

[2] The power-law fits to α and ν_0 shown in Fig. 2 work best for $\mathcal{N} \geq 2000$. For haloes resolved with fewer particles, the estimates of α and ν_0 are less accurate due to the small number of points available for the fit. There is a degeneracy in the fit parameters α and ν_0, since values with constant $\alpha\nu_0$ give similarly good fits. This introduces a large scatter in the two parameters around their mean trend with $\mathcal{N}$.

substructures. In total, the sample of haloes is missing a number of subhaloes with velocity ratio, ν, given by

$$n_{\rm hosts}\,(1-f(\nu))\,\widetilde{N}(\nu) = n_{\rm hosts}\,\frac{1-f(\nu)}{f(\nu)}\,\overline{N}(\nu), \qquad (8)$$

where $\widetilde{N}(\nu)$ and $\overline{N}(\nu)$ are the true and measured mean subhalo count (equation 5). To recover the true substructure count per halo, $\widetilde{N}(\nu)$, we add the missing subhaloes to the halo sample by randomly assigning each new subhalo to a host. We take the probability that a new subhalo is assigned to host halo, i, to be proportional to $1-f(\nu,\mathcal{N}_i)$, with $\mathcal{N}_i$ the number of particles in host halo i. The special case when the sample contains haloes of similar mass corresponds to each halo having equal weight, and so we distribute the missing substructures among the hosts with equal probability.

We apply the procedure above to samples of haloes within a narrow mass range and repeat the process independently for samples of haloes of different mass. This assumes that halo mass is the only factor that determines the subhalo count and ignores the effects of assembly bias. Previous studies have shown that the mean subhalo count depends on halo properties other than mass, like concentration and formation redshift (Gao et al. 2004; Zentner et al. 2005; Shaw et al. 2006; Gao et al. 2011), as well as on the large-scale environment of the host (Busha et al. 2011b; Cautun et al. 2014). Assembly bias can be taken into account by further restricting the halo samples to hosts with a given concentration or in a given environment. Neglecting assembly bias does not affect the ability of the method to recover the true mean subhalo count, but can result in a smaller value for the scatter in the count. We do not expect this effect to be significant since Gao et al. (2011) found that the dependence of the substructure number count on halo properties is not the main driver of the observed halo-to-halo scatter.

3.3 Evaluation of the extrapolation procedure

Fig. 3 shows how successful the extrapolation method is in recovering the mean, $\overline{N}(>\nu)$, and standard deviation, $\sigma(>\nu)$, of the subhalo population. The top panel gives the ratio, $\overline{N}_{\rm LR}(>\nu)/\overline{N}_{\rm HR}(>\nu)$, between the mean subhalo count found at low and high resolution as a function of the velocity ratio, ν. The middle panel gives the ratio, $\sigma_{\rm LR}(>\nu)/\sigma_{\rm HR}(>\nu)$, between the scatter in the subhalo counts found at low and high resolution. In both cases, a value of one corresponds to a successful recovery of the true mean and scatter in the number of subhaloes. We illustrate the result of the extrapolation method for host haloes resolved with $\sim 10^4$ (red circles) and $\sim 10^5$ (blue triangles) particles in the MS simulation. The two data sets show the comparison for haloes in the mass range (0.69–1.1) $\times\ 10^{13}\,h^{-1}\,{\rm M}_\odot$ and (0.35–1.2) $\times\ 10^{14}\,h^{-1}\,{\rm M}_\odot$, respectively, which were resolved at relatively low resolution in the MS and at higher resolution in the MS-II.

The bottom panel of Fig. 3 shows the completeness function, $f(\nu)$, of MS haloes resolved with $\sim 10^4$ and $\sim 10^5$ particles. For $f(\nu)=1$, there is no correction since the number of new subhaloes that need to be added is proportional to $(1-f(\nu))/f(\nu)$ (see equation 8). The correction becomes important only when $f(\nu)$ is significantly smaller than unity. The top panel of the figure shows that we obtain $\overline{N}_{\rm LR}(>\nu)/\overline{N}_{\rm HR}(>\nu)\approx 1$ down to values of ν equal to 0.14 and 0.09 for haloes resolved with $\sim 10^4$ and $\sim 10^5$ particles, respectively. These values of ν correspond to the range where $f(\nu)\gtrsim 0.15$ as may be seen by comparing to the bottom panel of the figure. Thus, our extrapolation method is successful at recovering the true mean subhalo number count as long as $f(\nu)\gtrsim 0.15$.

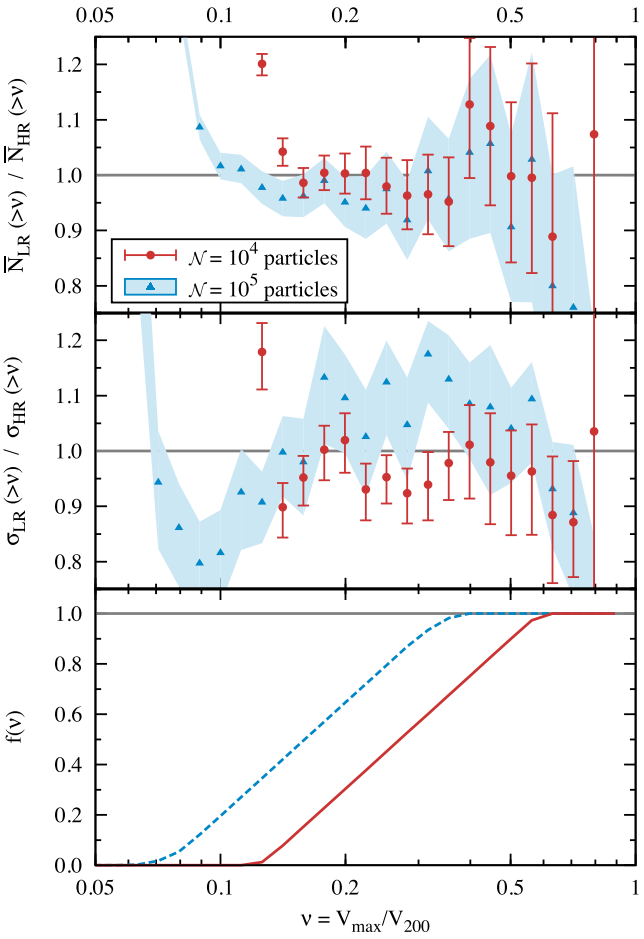

Figure 3. The effectiveness of our extrapolation method for subhalo statistics below the resolution limit of a simulation. The plots compare the mean, $\overline{N}(>\nu)$ (top), and scatter, $\sigma(>\nu)$ (middle) of the subhalo abundance in low- and high-resolution simulations. A value of one corresponds to a successful recovery of the mean and scatter. The low-resolution data are MS haloes resolved with $(0.8-1.2)\times 10^4$ (red circles) and $(0.4-1.2)\times 10^5$ (blue triangles) particles. The high-resolution data are MS-II haloes of corresponding mass. The error bars show the 1σ uncertainty in the determination of $\overline{N}(>\nu)$ and $\sigma(>\nu)$. The bottom panel shows the completeness function, $f(\nu)$, corresponding to the low-resolution halo samples: red for $\mathcal{N}\sim 10^4$ and dashed blue for $\mathcal{N}\sim 10^5$. The extrapolation procedure is applied only in the region $f(\nu)<1$; for $f(\nu)=1$ there are no additional subhaloes added.

For the scatter in the subhalo number count, we find from the centre panel of Fig. 3 that $\sigma_{\rm LR}(>\nu)/\sigma_{\rm HR}(>\nu)\approx 1$ down to values of ν of 0.16 and 0.11 for haloes resolved with $\sim 10^4$ and $\sim 10^5$ particles, respectively. Therefore, our extrapolation technique recovers the correct subhalo scatter in the region where $f(\nu)\gtrsim 0.3$. In the case of the second data set, we observe variations from unity of the order of 10 per cent. These are due to the small sample of only 70 MS-II haloes found in that mass range, which does not allow for a precise enough estimate of the scatter in the subhalo number count using bootstrap techniques. More importantly, we do not find any obvious systematic effects in the estimate of $\sigma(>\nu)$, except, at most, a 5 per cent lower than expected value for $f(\nu)\lesssim 0.5$. This implies that we can neglect subhalo assembly bias and still recover, to a good approximation, the true subhalo scatter. We also checked the effectiveness of the extrapolation procedure for the MS-II and *WMAP*7 simulations and found similar behaviour to the MS case presented here.

As a further test, we can compare the galactic mass haloes in the Aquarius simulations with their counterparts in the MS-II that have ∼1000 times fewer particles. With only six examples, it is not possible to carry out a statistical comparison but since the Aquarius haloes are resimulations of MS-II haloes we can perform an object-to-object comparison. This is shown in Fig. 4. We find that the ratio, $N_{\rm LR}(>\nu)/N_{\rm HR}(>\nu)$, between the low- and high-resolution results oscillates around one, without any obvious systematic trend. This shows that the extrapolation method faithfully recovers the statistics of the population over a large dynamical range in ν.

In Fig. 5, we show the values of ν above which we recover the true subhalo population with our extrapolation method. The solid curve gives the ν limit in the absence of extrapolation, given by the value of ν_0 for MS-II from Table 2. The dashed and dotted curves

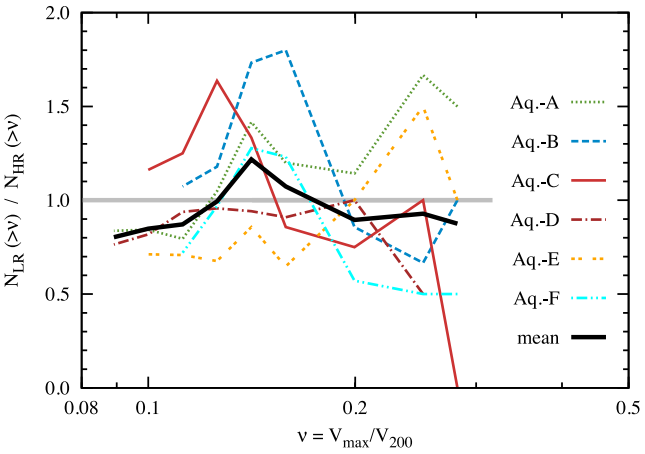

Figure 4. An object-to-object comparison of the subhalo count for the six Aquarius haloes, $N_{\rm HR}(>\nu)$, and the corrected subhalo count of their MS-II counterparts, $N_{\rm LR}(>\nu)$. The solid black line compares the mean substructure number in the two samples. The results reiterate that the extrapolation method gives the correct subhalo statistics although the scatter is appreciable for individual objects.

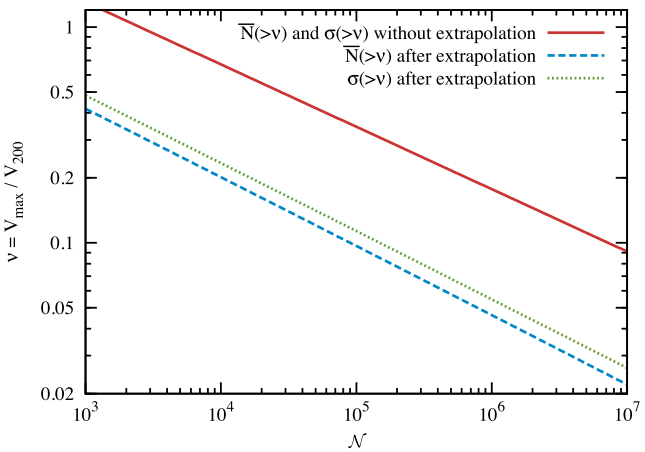

Figure 5. The lowest value of ν for which we recover the mean, $\overline{N}(>\nu)$, and the dispersion, $\sigma(>\nu)$, of the subhalo abundance. These limits are a function of the number of particles, $\mathcal{N}$, in the host halo. The solid curve gives the lower limits in the absence of extrapolation. The dashed and dotted curves represent the values of $\overline{N}(>\nu)$ and $\sigma(>\nu)$, respectively, when extrapolating below the resolution limit. While the results shown here are for MS-II, the other two simulations show a very similar behaviour, as may be seen in Fig. 2.

give the ν limits for the mean and dispersion in the subhalo number count when applying our extrapolation method. They were obtained by solving the $f(\nu) = 0.2$ and $f(\nu) = 0.3$ equations and correspond to conservative lower limits for recovering $\overline{N}(>\nu)$ and $\sigma(>\nu)$ as found in Fig. 3. By using our scaling method, we can estimate $\overline{N}(>\nu)$ and $\sigma(>\nu)$ to much lower ν values, corresponding to simulations with at least 50 times higher mass resolution.

4 THE ABUNDANCE OF SUBHALOES IN MW-MASS HALOES

4.1 Mean subhalo number

In this section, we investigate the subhalo distribution within haloes in the mass range $(0.6–2.2) \times 10^{12}\, h^{-1}\, {\rm M}_\odot$ to which we refer as MW-like or MW-mass host haloes. This mass range is consistent with estimates of the MW halo mass obtained through a variety of methods (Wilkinson & Evans 1999; Sakamoto et al. 2003; Battaglia et al. 2005; Dehnen et al. 2006; Smith et al. 2007; Li & White 2008; Xue et al. 2008; Gnedin et al. 2010; Guo et al. 2010; Watkins et al. 2010; Busha et al. 2011a; Piffl et al. 2014).

Using the extrapolation technique described in the previous section, we can recover the mean subhalo number, $\overline{N}(>\nu)$, for $\nu \geq 0.08$ (compared to $\nu \geq 0.3$ in MS-II and *WMAP*7 in the absence of these corrections). We illustrate this in Fig. 6 where we show the corrected $\overline{N}(>\nu)$ for MW-like hosts in the MS-II and *WMAP*7 simulations. The mean subhalo velocity function has a power-law dependence at small ν and an exponential cutoff at large ν. As BK10 did, we find that the function

$$N(>\nu) = \left(\frac{\nu}{\nu_1}\right)^a \exp\left(-\left(\frac{\nu}{\nu_{\rm cut}}\right)^b\right) \qquad (9)$$

gives a good match to the cumulative mean number of substructures as a function of ν for MW mass haloes. Following the prescription given by BK10, we fit the mean subhalo abundance for both MS-II and *WMAP*7. The resulting best-fitting parameters for the two simulations are given in Table 3. The best-fitting function fits the data very well, as may be seen in the middle panel of Fig. 6.

The MS-II and *WMAP*7 haloes have the same number of massive substructures, but there are important differences between the two simulations for low values of ν. The subhalo population in MS-II haloes has a slightly steeper slope and thus a higher abundance at low ν than in *WMAP*7 haloes. From the bottom panel of Fig. 6, it can be seen that for *WMAP*-7 cosmological parameters, MW-like haloes have only 93 and 86 per cent of the MS-II subhaloes at $\nu = 0.2$ and $\nu = 0.1$, respectively.

When comparing with results in the literature, we find that other studies have systematically underestimated the substructure abundance at low ν as a result of not taking finite resolution effects properly into account. Thus, while BK10 found similar values for the $\nu_{\rm cut}$ and b fit parameters for MS-II subhaloes, they underestimated the slope of the velocity function at low ν: they find $a = -2.98$ whereas for substructures within R_{100} we find $a = -(3.22 \pm 0.09)$. The discrepancy in slope is due to BK10 fitting the subhalo count down to $\nu = 0.2$, while we find that without proper correction, the MS-II simulation gives the correct subhalo abundance only for $\nu \geq 0.3$. In contrast, Wang12 found a slope of $a = -3.11$ within R_{200}, which agrees within the errors with our value of $a = -(3.17 \pm 0.09)$, but nevertheless they find 20 per cent fewer subhaloes within R_{200} at all values of ν.

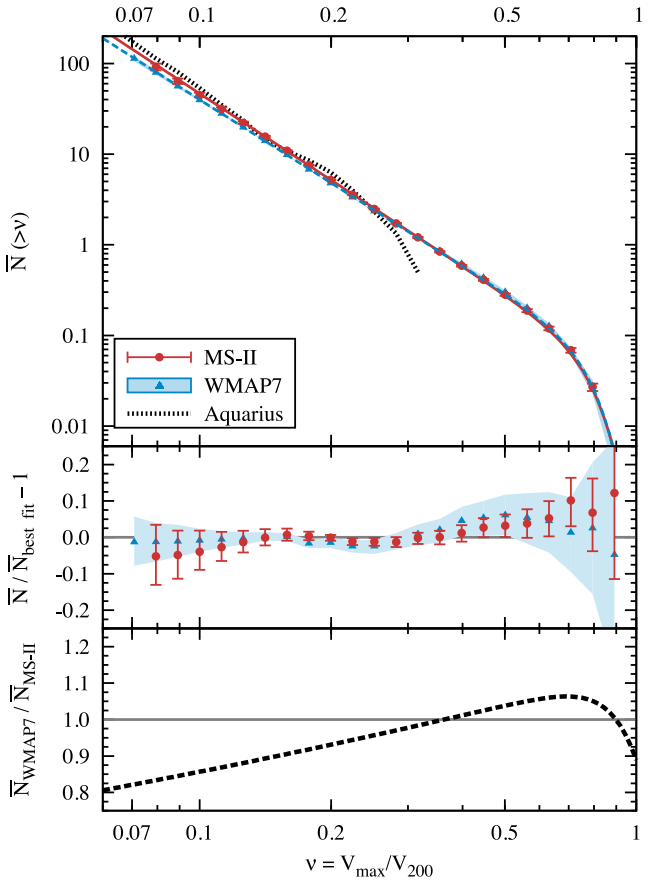

Figure 6. Top: the corrected mean subhalo count as a function of the velocity ratio, ν, in MW-mass haloes in the MS-II and *WMAP7* simulations. The two lines show the best-fitting function given by equation (9) for MS-II (solid red) and *WMAP7* (dashed blue). The dotted curve shows $\overline{N}(>\nu)$ for the six Aquarius haloes. Middle: the ratio between the actual number of subhaloes in the simulations and the number given by the best-fitting function to the data in the top panel. The errors bars give the 1σ error in the estimate of $\overline{N}(>\nu)$ due to finite sample effects (which dominate for $\nu > 0.3$) and due to uncertainties in the estimate of the completeness function (which dominate for $\nu < 0.2$). Bottom: ratio of the best-fitting function to the subhalo abundance in the MS-II and *WMAP7* simulations.

Table 3. The best-fitting parameters of equation (9) for the mean subhalo number count in MW-like haloes in the MS-II and *WMAP7* simulations, within both R_{200} and R_{100} from the host halo centre. The 1σ errors in the fit are at most, $\Delta a = 0.02$, $\Delta\nu_1 = 0.003$, $\Delta b = 1$ and $\Delta\nu_{\rm cut} = 0.02$. The value of the parameter a is sensitive to errors in the estimate of the completeness function (see Table 2), which introduces an additional systematic error of $\Delta a = 0.07$.

Simulation	Subhaloes within	a	ν_1	b	$\nu_{\rm cut}$
MS-II	R_{200}	−3.17	0.338	7	0.80
WMAP7		−3.05	0.336	7	0.79
MS-II	R_{100}	−3.22	0.366	7	0.80
WMAP7		−3.12	0.364	7	0.79

The main difference between Wang12 and BK10 is that, just as we have done, Wang12 used the invariance of $\overline{N}(>\nu)$ with host halo mass to estimate the average subhalo abundance. This approach appears to give the correct value for the slope, a. However, as BK10 did, Wang12 overestimated the value of ν at which resolution effects become important and their fits to $\overline{N}(>\nu)$ included host haloes for which only ∼75 per cent of substructures are detected. Another difference with these studies is that we use a phase-space halo finder while both BK10 and Wang12 use a configuration-space halo finder. However, we expect that this choice accounts for at most a few per cent of the difference, as we show in Appendix B.

4.2 Scatter in the substructure population

The dispersion of the subhalo number distribution characterizes halo-to-halo variations and is important not only for quantifying how typical the MW and its satellites are, but also for the interpretation of conclusions derived from very high resolution simulations of a few MW-sized haloes (Diemand et al. 2008; Springel et al. 2008; Stadel et al. 2009). The scatter in the subhalo abundance is also an important parameter when applying halo occupation distribution (HOD) models to populate DM haloes with galaxies (e.g. Benson et al. 2000; Ma & Fry 2000; Peacock & Smith 2000; Seljak 2000; Scoccimarro et al. 2001; Berlind & Weinberg 2002).

We find that, at large ν, the scatter in the substructure abundance matches the dispersion of a Poisson distribution with the same mean. At lower velocity ratios, as the average number of subhaloes increases, we find a much larger scatter than expected for a Poisson distribution. This is illustrated in Fig. 7 that shows the ratio of the measured subhalo scatter to the dispersion, $\overline{N}^{1/2}(>\nu)$, of a Poisson distribution with mean $\overline{N}(>\nu)$. We find that the standard deviation, $\sigma(>\nu)$, in both the MS-II and *WMAP7* subhalo distributions has the same dependence on ν that can be parametrized as

$$\sigma(>\nu) = \overline{N}^{1/2}(>\nu) \begin{cases} 1 & \nu \geq \nu_\sigma \\ 1 + \beta \ln^2(\nu/\nu_\sigma) & \nu < \nu_\sigma . \end{cases} \quad (10)$$

Fitting this equation to the data, we find $\nu_\sigma = 0.50$ and $\beta = 0.11$. This fit is a very good match to the subhalo abundance scatter, as may be seen in Fig. 7. The scatter for substructures within R_{100} from the host halo centre shows a similar functional form, but with best-fitting parameters $\nu_\sigma = 0.55$ and $\beta = 0.14$.

Our result that the scatter in the number of small substructures differs significantly from the Poissonian expectation is in good

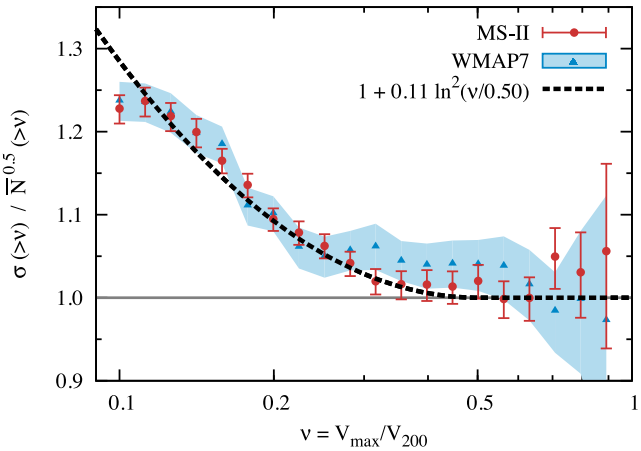

Figure 7. The dependence of the scatter in the subhalo abundance, $\sigma(>\nu)$, on the velocity ratio, ν, for MW-like hosts. For clarity, we show $\sigma(>\nu)/\overline{N}^{1/2}(>\nu)$, the ratio between the observed scatter and the Poisson value, $\overline{N}^{1/2}(>\nu)$. The dashed black curve gives the fit to the data for both the MS-II and *WMAP7* simulations, with the best-fitting parameters quoted in the legend. The error bars represent the 1σ error in $\sigma(>\nu)$.

agreement with previous results: Benson et al. (2000) showed that the occupation of haloes by galaxies is not a Poisson process and BK10 showed that the dispersion in the number of subhaloes above a certain mass is a combination of Poisson scatter at the HM end and larger than Poisson scatter at the low-mass (LM) end.

4.3 Subhalo occupation distribution

Since the scatter in the subhalo population is significantly non-Poissonian, we follow BK10 and Busha et al. (2011b), and model the probability distribution function (PDF) of the number of substructures with a given value of ν using the negative binomial distribution (NBD),

$$P(N|r,s) = \frac{\Gamma(N+r)}{\Gamma(r)\Gamma(N+1)} s^r (1-s)^N, \tag{11}$$

where N is the number of subhaloes per halo, $\Gamma(x) = (x-1)!$ is the Gamma function, which, for integer values of x, reduces to the factorial function, and r and s are two parameters. The mean and dispersion of this distribution can be computed analytically in terms of r and s. The inverse holds too, with the two distribution parameters given by

$$r = \frac{\mu^2}{\sigma^2 - \mu}, \qquad s = \frac{\mu}{\sigma^2}, \tag{12}$$

where μ and σ denote the mean and dispersion of the NBD. Thus, μ and σ completely specify the distribution. The NBD has also been used to describe the number of satellite galaxies in HOD models (e.g. Berlind & Weinberg 2002).

BK10 found that the NBD gives a better fit to the substructure population than a Poisson distribution when counting all subhaloes containing more than a certain fraction of the host mass. We find that the NBD also matches well the substructure PDF when counting all subhaloes with velocity ratios larger than ν. This is illustrated in Fig. 8 where we plot the subhalo occupation distribution for MW-mass hosts in both the MS-II and *WMAP7* simulations. The solid and dashed lines NBDs. These are not fits to the data points, but are obtained from equation (12) using the mean subhalo number, $\overline{N}(>\nu)$, from equation (9) and the dispersion, $\sigma(>\nu)$, from equation (10). It is clear in the figure that the NBD reproduces very well the subhalo distribution at all values of ν. Therefore, knowing the mean and scatter of the subhalo number counts is enough to infer the full PDF.

The grey line in the lower panel of Fig. 8 shows a Poisson distribution with the same mean as the MS-II subhalo abundance. It is clear that the Poisson distribution severely underestimates the tails of the PDF. Thus, even a modest increase in the dispersion compared to the Poisson case (25 per cent at $\nu = 0.1$) leads to large deviations from a Poisson distribution.

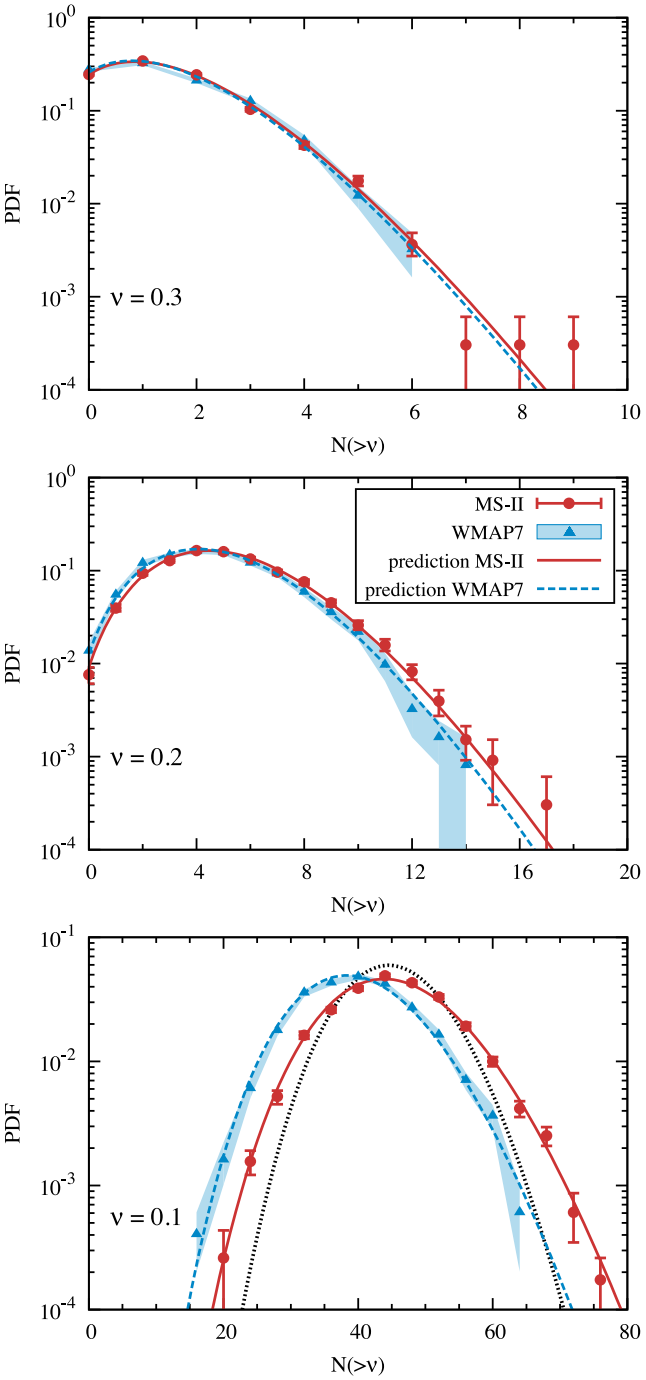

Figure 8. The PDF of the number of substructures in MW-like host haloes with $\nu \geq 0.3$ (top), $\nu \geq 0.2$ (middle) and $\nu \geq 0.1$ (bottom). The solid and dashed curves show the NBD with the mean and standard deviation found in Figs 6 and 7. The solid grey curve in the bottom panel shows a Poisson distribution with the same mean as the MS-II haloes.

5 DEPENDENCE OF SUBHALO NUMBER ON HOST MASS

In Fig. 9, we investigate how the mean number of substructures as a function of normalized velocity, ν, varies for hosts of different mass. To emphasize the differences, we normalize the mean subhalo number count in each mass bin by the mean, $\overline{N}_{\rm MW-mass}(>\nu)$, for MW-mass hosts. We find that for $\nu \leq 0.3$ there is very little dependence on host halo mass, with at most a 5 per cent difference between MW-like and cluster sized haloes. In contrast, for larger subhaloes we find a complex variation with host mass that can be split in the two regimes. Substructures with $\nu \gtrsim 0.8$ tend to be much more common in lower mass haloes than in HM ones. Thus, it is much more likely to find a halo–subhalo pair of similar mass in MW-like and lower mass hosts than in cluster sized objects. In the $0.3 \lesssim \nu \lesssim 0.7$ range this trend is reversed, with more subhaloes present in massive hosts than in less massive ones. In this case, the increase of $\overline{N}(>\nu)$ with the mass of the host is small, with $\sim$15 per cent variation in the number of substructures per decade of host halo mass.

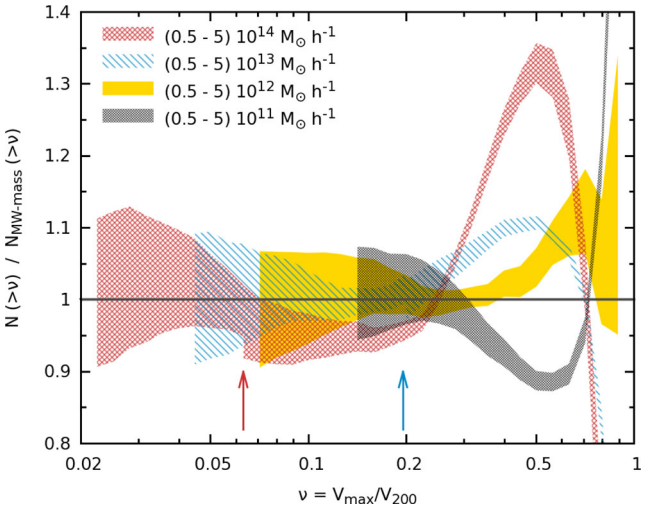

Figure 9. The dependence of the abundance of substructures as a function of ν, $N(>\nu)$, on the host halo mass. To emphasize the differences, we divide by the mean subhalo number, $\overline{N}_{\rm MW-mass}(>\nu)$, for MS-II MW-like hosts. The two vertical arrows indicate the ν value where we switch from MS to MS-II data for hosts of mass (0.5–5) $\times\ 10^{14}\,h^{-1}\,{\rm M}_\odot$ (red arrow) and (0.5–5) $\times\ 10^{13}\,h^{-1}\,{\rm M}_\odot$ (blue arrow). The other two mass bins show only MS-II haloes. The width of each curve shows the 1σ error in the determination of $N(>\nu)$.

The results in Fig. 9 support the assumption we made in Section 3 that the mean subhalo count as a function of ν varies only slowly or not at all with host halo mass. This explains why method B works is valid for estimating the completeness function. This also means that our results for the subhalo population of MW-like haloes are insensitive to the exact mass range used to define MW-mass haloes. The invariance of the mean substructure count on host mass makes it possible to use host haloes of all masses to compute $\overline{N}(>\nu)$, but only for $\nu \leq 0.3$. This property was already exploited by Wang12, who used haloes in a large mass range to investigate the subhalo population of MW-like haloes and derive constraints on the MW halo mass.

The number of subhaloes is independent of host halo mass only when expressed in terms of the ratio $\nu = V_{\rm max}^{\rm subhalo}/V_{200}^{\rm host}$. Previous studies have shown that there is a variation with host halo mass when considering $\overline{N}(>M^{\rm subhalo}/M^{\rm host})$ (Gao et al. 2004, 2011; Zentner et al. 2005) or $\overline{N}(>V_{\rm max}^{\rm subhalo}/V_{\rm max}^{\rm host})$ (Busha et al. 2011b; Klypin et al. 2011).

6 THE MW MASSIVE SATELLITES

As we discussed in Section 1, the conclusion that the MW has at most three satellites residing in substructures with $V_{\rm max} \geq 30\,{\rm km\,s^{-1}}$ – the two Magellanic Clouds and the Sagittarius dwarf – seems at odds with the number of such substructures, eight on average, found in the Aquarius simulations of haloes of mass $M_{200} \sim 2 \times 10^{12}\,h^{-1}\,{\rm M}_\odot$ (Boylan-Kolchin et al. 2011). The probability of finding such a population of substructures within ΛCDM was investigated by Wang12 who found that this 'too-big-to-fail-problem' is only present if the MW halo has a mass similar to the Aquarius haloes, but the problem is avoided altogether if the halo mass is a factor of 2 smaller. They were therefore able to set an upper limit to the MW halo mass under the assumption that ΛCDM is the correct model. Since we find a higher number of substructures than Wang12 did, we now re-examine how their constraints on the MW mass change when using the subhalo statistics derived in Section 4.

Given a halo of virial velocity, V_{200}, the probability that it hosts at most X substructures with $V_{\rm max} \geq V_0$ is given by

$$p(\leq X, V_0) = \sum_{k=0}^{X} P(k|r(>\nu), s(>\nu)) \quad \text{with } \nu = \frac{V_0}{V_{200}}\,, \tag{13}$$

where $P(k|r(>\nu), s(>\nu))$ is the NBD that gives the probability that a halo has k subhaloes with velocity ratio larger than ν (see equation 11). The distribution parameters, $r(>\nu)$ and $s(>\nu)$, are uniquely determined by the mean and scatter of the subhalo population through equation (12).

The probability, $p(\leq 3, 30\,{\rm km\,s^{-1}})$, is shown in Fig. 10 as a function of halo virial velocity (lower tick marks) or, equivalently, halo mass (upper tick marks). The results shown are for subhaloes identified within R_{100}, which is close to the maximum distance at which dwarf galaxies are identified as being MW satellites. The solid blue curve shows $p(\leq 3, 30\,{\rm km\,s^{-1}})$ from the MS-II simulation. The probability is a steep function of host halo mass, decreasing from ∼70 per cent at $0.5 \times 10^{12}\,{\rm M}_\odot$ to ∼15 per cent at $1 \times 10^{12}\,{\rm M}_\odot$, and becomes negligible for haloes more massive than $2 \times 10^{12}\,{\rm M}_\odot$. For convenience, we give values of $p(\leq 3, 30\,{\rm km\,s^{-1}})$ in Table 4 for some suggestive halo masses. Therefore, assuming that the ΛCDM cosmology is the correct model, given that the MW has only three satellites with $V_{\rm max} \geq 30\,{\rm km\,s^{-1}}$ it is unlikely that our galaxy's halo is more massive than $\sim 1.5 \times 10^{12}\,{\rm M}_\odot$.

The dashed orange curve in Fig. 10 shows results for a ΛCDM model with *WMAP*-7 parameters. Since this model has fewer substructures at low ν than a model with *WMAP*-1 parameters, then, at fixed halo mass, it has a higher $p(\leq 3, 30\,{\rm km\,s^{-1}})$ resulting in a weaker upper limit on the MW halo mass. Nevertheless, because of the steep decline of the probability with halo mass, the upper

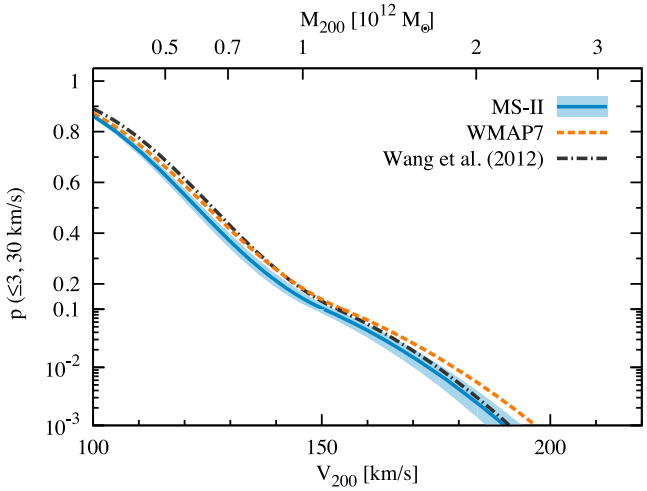

Figure 10. The probability, $p(\leq 3, 30\,{\rm km\,s^{-1}})$, that a halo has at most three substructures with $V_{\rm max} \geq 30\,{\rm km\,s^{-1}}$ within a distance R_{100} from its centre. The probability is given as a function of halo virial velocity, V_{200} (lower tick marks), and halo mass, M_{200} (upper tick marks). We show results for both the *WMAP*-1 cosmology used in MS-II (solid line) as well as for the more recent *WMAP*-7 parameters (dashed line). The dash–dotted line shows the results of Wang12. The width of the MS-II curve gives the 1σ error due to uncertainties in the subhalo abundance of galactic haloes. The *WMAP*7 results have the same error associated with them (not shown). Note that the y-axis is linear above 0.1 and logarithmic for lower values.

Table 4. The probability, $p(\leq 3, 30\,\mathrm{km\,s^{-1}})$, of finding three or fewer substructures with $V_{\rm max} \geq 30\,\mathrm{km\,s^{-1}}$ for suggestive halo masses. Predictions are given for two choices of cosmological parameters derived from the *WMAP*-1 and *WMAP*-7 data, and they are compared to the previous results by Wang12 that are based on *WMAP*-1 parameters.

Halo mass	($\times 10^{12}\,\mathrm{M}_\odot$)	0.5	0.7	1	2
WMAP-1	(%)	67	38	13	0.2
WMAP-7	(%)	72	44	20	0.6
Wang12	(%)	76	48	22	0.3

limit on the MW halo mass is only slightly increased in this model compared to the one with *WMAP*-1 parameters.

We expect that our results are robust to changes in cosmological parameters, especially concerning the recent Planck Collaboration (2013) measurement. The subhalo abundance could potentially be affected by the change in the concentration of haloes and subhaloes, but Dutton & Macciò (2014) showed that the increase in $\Omega_{\rm m}$ between the *WMAP*-1 and Planck measurements is balanced by the decrease in the values of σ_8, n_s and h, such that haloes of the same mass have the same concentration in both cosmologies. In addition, increasing $\Omega_{\rm m}$ leads to a larger number of haloes at fixed mass and potentially to more subhaloes, but, despite all this, the scaled subhalo velocity function is insensitive to variations in $\Omega_{\rm m}$ (Garrison-Kimmel et al. 2014).

Compared to the previous results of Wang12, we find stricter upper limits for the mass of the MW halo. This is seen in Fig. 10 by comparing the solid and dash–dotted curves, with both corresponding to *WMAP*-1 parameters. The main cause of the discrepancy is that Wang12 found up to 20 per cent fewer substructures than we find (see 4.1) and thus overestimated the probability at fixed halo mass. A second source of disagreement is the PDF used to model the subhalo population. Wang12 used a Poisson distribution that underestimates the true tails of the subhalo number distribution (see Fig. 8 for an example). This effect becomes important when dealing with low $p(\leq 3, 30\,\mathrm{km\,s^{-1}})$ values and leads to an underestimate of the true probability. This is the reason why the Wang12 probability for $M_{200} \gtrsim 10^{12}\,\mathrm{M}_\odot$ is lower than our value for *WMAP*-7 parameters, even though we find a larger subhalo count in the latter case.

7 HOW TYPICAL ARE THE AQUARIUS HALOES?

In view of the prominence that the Aquarius halo simulations have had, particularly in the work of Springel et al. (2008) and Boylan-Kolchin et al. (2011, 2012), it is interesting to ask how typical these haloes are of the global population of haloes of similar mass. BK10 addressed this question in some detail using the MS-II and found that the six Aquarius haloes are representative in so far as the properties that they considered (such as assembly history and internal structure) is concerned. However, they did not consider the distribution of ν that is of most interest here.

In Fig. 11, we compare the cumulative ν distribution, $N(>\nu)$, of each of the six level-2 Aquarius haloes with that of the population of MS-II haloes in the mass range (0.6–2.2) $\times\ 10^{12}\,h^{-1}\,\mathrm{M}_\odot$. To show the differences more clearly, we normalize the distributions to the mean, $\overline{N}_{\rm MW-mass}(>\nu)$, of the MS-II. The thick dashed line shows the median for the MS-II population, which is always smaller

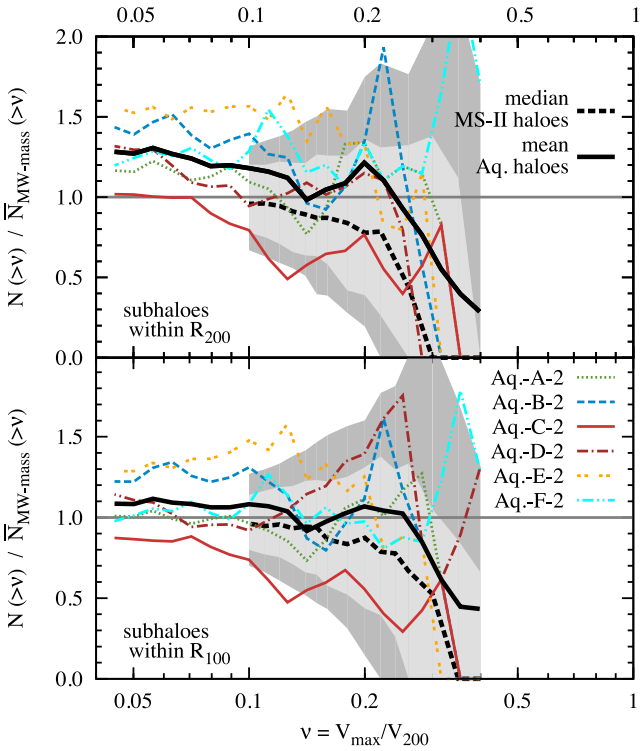

Figure 11. The cumulative distribution, $N(>\nu)$, of normalized velocities in each of the six level-2 Aquarius haloes compared with that of the global population of haloes in the mass range (0.6–2.2) $\times\ 10^{12}\,h^{-1}\,\mathrm{M}_\odot$ in the MS-II. The Aquarius data are normalized to the mean, $\overline{N}_{\rm MW-mass}(>\nu)$, in the MS-II. The top and bottom panels show results for substructures within distance R_{200} and R_{100} from the host halo centre, respectively. The thick dashed curve shows the median of the MS-II population while the light shaded region delimits the 16 and 84 percentiles of the distribution and the dark shaded region the 5 and 95 percentiles. We restrict our analysis to $\nu \leq 0.4$, since only Aq.-F has subhaloes with higher ν.

than the mean count due to the long tail in the subhalo number PDF (see Fig. 8). The light and dark shaded regions show the 68 and 90 per cent scatter around the median obtained by modelling the subhalo distribution function as an NBD with the mean and dispersion values given in Section 4.

Our comparison of the Aquarius and MS-II subpopulations is restricted to $\nu \geq 0.1$, the resolution limit for MS-II subhaloes. For completeness, we present the substructure function of the Aquarius haloes down to their resolution limit, $\nu \geq 0.04$, but we do not use the additional range in the comparison with the MS-II.

Fig. 11 shows that the six Aquarius haloes have a subhalo normalized velocity function that is in good agreement with the much larger sample of MS-II haloes of similar mass, both when considering subhaloes within R_{200} (top panel) and within R_{100} (bottom panel). The mean of the Aquarius velocity function lies well within the 68 per cent scatter and it is in very good agreement with the mean in the MS-II. Individually, we find that Aq.-C has the smallest number of subhaloes compared to the other Aquarius haloes, especially for $\nu \leq 0.25$, but it is still within the MS-II distribution. The remaining five Aquarius haloes have a substructure velocity function similar or larger than the median for the MS-II haloes. This result agrees with Wang12 who found that five of the Aquarius haloes have more substructures with $V_{\rm max} \geq 30\,\mathrm{km\,s^{-1}}$ than the mean.

To summarize, for $\nu \lesssim 0.25$, five out of the six Aquarius haloes have a subhalo normalized velocity function that is similar or larger than the median for a representative sample of MW-mass haloes. This needs to be born in mind when comparing the small number of massive satellites present in the MW with the Aquarius haloes, especially if, as seems to be the case according to determinations of the satellite luminosity function in the SDSS (Guo et al. 2012; Wang & White 2012), our galaxy has significantly fewer satellites than average.

8 SUMMARY

We have introduced an extrapolation method to infer subhalo number statistics below the resolution limit of a cosmological simulation. This method statistically generates the correct subhalo abundance from the partial information available in a simulation of limited resolution. We have tested this technique by comparing results of simulations of different resolution – including the high-resolution Aquarius simulations – and conclude that it extends the subhalo number counts correctly down to what would be found in a simulation of 50 times or more better mass resolution. The technique reproduces only the statistics of the subhalo population, not the position or structure of subhaloes. We characterized the subhalo abundance in terms of the scaled subhalo velocity function, $\overline{N}(>\nu)$, which gives the number of substructures above $\nu = V_{\rm max}/V_{200}$, where $V_{\rm max}$ is the subhalo maximum circular velocity and V_{200} the virial velocity of the host. We give a fitting formula for the completeness function as a function of ν that can be used to extrapolate the results of a simulation.

As noted by BK10 and Busha et al. (2011b), the PDF of the number of substructures with a given value of ν is well described by a NBD. Thus, the substructure occupation distribution can be obtained given only the mean and dispersion of the subhalo number count. The scatter in the number counts becomes distinctly non-Poissonian for $\nu \leq 0.3$, so simply assuming a Poisson distribution will greatly underestimate the tails of the ν subhalo distribution.

We applied our technique to the Millennium and Millennium-II (MS-II) simulations and to a simulation of similar volume, but lower resolution, with *WMAP*-7 cosmological parameters (rather than the *WMAP*-1 values of the MS-II). We focused on haloes of mass similar to the MW but our results are insensitive to the exact halo mass range assumed for the MW since the scaled subhalo velocity function is insensitive to mass for $\nu \leq 0.3$; for larger values of ν, it shows a weak trend with host halo mass. This confirms, and extends to a much larger dynamic range, the results of Wang12 (see also Moore et al. 1999; Kravtsov et al. 2004; Zheng et al. 2005; Springel et al. 2008; Weinberg et al. 2008).

As BK10, we found that the mean cumulative subhalo number count, $\overline{N}(>\nu)$, in haloes of mass similar to the MW in the MS-II is well described by a power law with an exponential cutoff. The number of small mass substructures depends slightly on the cosmological parameters: it is lower for *WMAP*-7 than for *WMAP*-1 parameters,

We showed that the substructure population in haloes of mass similar to the MW in the MS-II is complete only to $\nu \sim 0.3$, which corresponds to satellites with $V_{\rm max} \sim 45\,{\rm km\,s^{-1}}$. By contrast, our extrapolation method gives accurate results for the mean and scatter of substructures in these MS-II haloes for $\nu \geq 0.1$, which corresponds to $V_{\rm max} \sim 15\,{\rm km\,s^{-1}}$. Previous studies optimistically estimated that this subhalo population is complete down to $\nu \sim 0.2$. BK10 found ∼15 per cent fewer subhaloes than us for $\nu \leq 0.2$. Exploiting the approximate scale-invariance of $\overline{N}(>\nu)$, Wang12 estimated the number of subhaloes in MW-mass haloes over a large range of ν. However, they found 20 per cent fewer substructures at all ν than we do because the ν function is dominated by the LM subhaloes for which they recover only ∼75 per cent of the population.

Wang12 used their inferred ν distribution of subhaloes in MW-mass haloes and the fact that, as highligthed by Boylan-Kolchin et al. (2011, 2012), the MW has only a very small number of massive satellites to set an upper limit on the MW mass under the assumption that ΛCDM is the correct cosmological model. Since we find fewer substructures in these haloes than Wang12 did, we revisited their argument and calculated the probability for a halo to have a similar population of massive substructure as the MW, i.e. three or fewer substructures with $V_{\rm max} \geq 30\,{\rm km\,s^{-1}}$, as a function of the halo's mass. We were then able to set a stricter upper bound on the MW mass than found by Wang12: the probability of having the observed number of large subhaloes is 20 per cent for $1 \times 10^{12}\,{\rm M}_\odot$ mass haloes and practically zero for haloes more massive than $2 \times 10^{12}\,{\rm M}_\odot$.

Finally, we investigated how typical the subhalo population of the Aquarius haloes (Springel et al. 2008) is compared to those of the global population of haloes of similar mass in the MS-II. We find that the Aquarius haloes fall within the scatter of the MS-II population but only one of the six Aquarius examples has fewer subhaloes than the median of the MW-mass haloes in the MS-II. This needs to be born in mind when using the Aquarius subhaloes to draw general conclusions about our halo.

ACKNOWLEDGEMENTS

We are grateful to the referee's comments that have improved this paper. This work was supported in part by ERC Advanced Investigator grant COSMIWAY [grant number GA 267291] and the Science and Technology Facilities Council [grant number ST/F001166/1, ST/I00162X/1]. WAH is also supported by the Polish National Science Center [grant number DEC-2011/01/D/ST9/01960]. RvdW acknowledges support by the John Templeton Foundation, grant number FP05136-O. The simulations used in this study were carried out by the Virgo consortium for cosmological simulations. Additional data analysis was performed on the Cosma cluster at ICC in Durham and on the Gemini machines at the Kapteyn Astronomical Institute in Groningen.

This work used the DiRAC Data Centric system at Durham University, operated by ICC on behalf of the STFC DiRAC HPC Facility (www.dirac.ac.uk). This equipment was funded by BIS National E-infrastructure capital grant ST/K00042X/1, STFC capital grant ST/H008519/1, and STFC DiRAC Operations grant ST/K003267/1 and Durham University. DiRAC is part of the National E-Infrastructure. This research was carried out with the support of the 'HPC Infrastructure for Grand Challenges of Science and Engineering' Project, co-financed by the European Regional Development Fund under the Innovative Economy Operational Programme.

REFERENCES

Battaglia G. et al., 2005, MNRAS, 364, 433
Behroozi P. S., Wechsler R. H., Wu H.-Y., 2013, ApJ, 762, 109
Benson A. J., Cole S., Frenk C. S., Baugh C. M., Lacey C. G., 2000, MNRAS, 311, 793
Benson A. J., Lacey C. G., Baugh C. M., Cole S., Frenk C. S., 2002a, MNRAS, 333, 156

Benson A. J., Frenk C. S., Lacey C. G., Baugh C. M., Cole S., 2002b, MNRAS, 333, 177
Berlind A. A., Weinberg D. H., 2002, ApJ, 575, 587
Boylan-Kolchin M., Springel V., White S. D. M., Jenkins A., Lemson G., 2009, MNRAS, 398, 1150
Boylan-Kolchin M., Springel V., White S. D. M., Jenkins A., 2010, MNRAS, 406, 896 (BK10)
Boylan-Kolchin M., Bullock J. S., Kaplinghat M., 2011, MNRAS, 415, L40
Boylan-Kolchin M., Bullock J. S., Kaplinghat M., 2012, MNRAS, 422, 1203
Bullock J. S., Kravtsov A. V., Weinberg D. H., 2000, ApJ, 539, 517
Busha M. T., Marshall P. J., Wechsler R. H., Klypin A., Primack J., 2011a, ApJ, 743, 40
Busha M. T., Wechsler R. H., Behroozi P. S., Gerke B. F., Klypin A. A., Primack J. R., 2011b, ApJ, 743, 117
Cautun M., Frenk C. S., van de Weygaert R., Hellwing W. A., Jones B. J. T., 2014, preprint (arXiv:1405.7697)
Clocchiatti A. et al., 2006, ApJ, 642, 1
Cole S. et al., 2005, MNRAS, 362, 505
Davis M., Efstathiou G., Frenk C. S., White S. D. M., 1985, ApJ, 292, 371
Dehnen W., McLaughlin D. E., Sachania J., 2006, MNRAS, 369, 1688
Diemand J., Kuhlen M., Madau P., Zemp M., Moore B., Potter D., Stadel J., 2008, Nature, 454, 735
Dutton A. A., Macciò A. V., 2014, MNRAS, 441, 3359
Gao L., White S. D. M., Jenkins A., Stoehr F., Springel V., 2004, MNRAS, 355, 819
Gao L., Frenk C. S., Boylan-Kolchin M., Jenkins A., Springel V., White S. D. M., 2011, MNRAS, 410, 2309
Garrison-Kimmel S., Horiuchi S., Abazajian K. N., Bullock J. S., Kaplinghat M., 2014, MNRAS, 444, 961
Gnedin O. Y., Brown W. R., Geller M. J., Kenyon S. J., 2010, ApJ, 720, L108
Guo Q., White S., Li C., Boylan-Kolchin M., 2010, MNRAS, 404, 1111
Guo Q., Cole S., Eke V., Frenk C., 2012, MNRAS, 427, 428
Guy J. et al., 2010, A&A, 523, A7
Jiang F., van den Bosch F. C., 2014, preprint (arXiv:1403.6827)
Karachentsev I. D., Karachentseva V. E., Huchtmeier W. K., Makarov D. I., 2004, AJ, 127, 2031
Klypin A., Kravtsov A. V., Valenzuela O., Prada F., 1999, ApJ, 522, 82
Klypin A. A., Trujillo-Gomez S., Primack J., 2011, ApJ, 740, 102
Knebe A. et al., 2011, MNRAS, 415, 2293
Komatsu E. et al., 2011, ApJS, 192, 18
Kravtsov A. V., Berlind A. A., Wechsler R. H., Klypin A. A., Gottlöber S., Allgood B., Primack J. R., 2004, ApJ, 609, 35
Li Y.-S., White S. D. M., 2008, MNRAS, 384, 1459
Łokas E. L., 2009, MNRAS, 394, L102
Ma C.-P., Fry J. N., 2000, ApJ, 543, 503
Moore B., Governato F., Quinn T., Stadel J., Lake G., 1998, ApJ, 499, L5
Moore B., Ghigna S., Governato F., Lake G., Quinn T., Stadel J., Tozzi P., 1999, ApJ, 524, L19
Onions et al., 2012, MNRAS, 423, 1200
Peacock J. A., Smith R. E., 2000, MNRAS, 318, 1144
Peñarrubia J., McConnachie A. W., Navarro J. F., 2008, ApJ, 672, 904
Piffl T. et al., 2014, A&A, 562, A91
Planck Collaboration et al., 2013, preprint (arXiv:1303.5076)
Purcell C. W., Zentner A. R., 2012, J. Cosmol. Astropart. Phys., 12, 7
Sakamoto T., Chiba M., Beers T. C., 2003, A&A, 397, 899
Sawala T., Frenk C. S., Crain R. A., Jenkins A., Schaye J., Theuns T., Zavala J., 2013, MNRAS, 431, 1366
Scoccimarro R., Sheth R. K., Hui L., Jain B., 2001, ApJ, 546, 20
Seljak U., 2000, MNRAS, 318, 203
Shaw L. D., Weller J., Ostriker J. P., Bode P., 2006, ApJ, 646, 815
Smith M. C. et al., 2007, MNRAS, 379, 755
Somerville R. S., 2002, ApJ, 572, L23
Spergel D. N. et al., 2003, ApJS, 148, 175
Springel V., White S. D. M., Tormen G., Kauffmann G., 2001, MNRAS, 328, 726
Springel V. et al., 2005, Nature, 435, 629
Springel V. et al., 2008, MNRAS, 391, 1685
Stadel J., Potter D., Moore B., Diemand J., Madau P., Zemp M., Kuhlen M., Quilis V., 2009, MNRAS, 398, L21
Strigari L. E., Bullock J. S., Kaplinghat M., Simon J. D., Geha M., Willman B., Walker M. G., 2008, Nature, 454, 1096
Strigari L. E., Frenk C. S., White S. D. M., 2010, MNRAS, 408, 2364
Vera-Ciro C. A., Helmi A., Starkenburg E., Breddels M. A., 2013, MNRAS, 428, 1696
Walker M. G., Mateo M., Olszewski E. W., Peñarrubia J., Wyn Evans N., Gilmore G., 2009, ApJ, 704, 1274
Wang W., White S. D. M., 2012, MNRAS, 424, 2574
Wang J., Frenk C. S., Navarro J. F., Gao L., Sawala T., 2012, MNRAS, 424, 2715 (Wang12)
Watkins L. L., Evans N. W., An J. H., 2010, MNRAS, 406, 264
Weinberg D. H., Colombi S., Davé R., Katz N., 2008, ApJ, 678, 6
Wilkinson M. I., Evans N. W., 1999, MNRAS, 310, 645
Wolf J., Martinez G. D., Bullock J. S., Kaplinghat M., Geha M., Muñoz R. R., Simon J. D., Avedo F. F., 2010, MNRAS, 406, 1220
Xue X. X. et al., 2008, ApJ, 684, 1143
Zentner A. R., Berlind A. A., Bullock J. S., Kravtsov A. V., Wechsler R. H., 2005, ApJ, 624, 505
Zheng Z. et al., 2005, ApJ, 633, 791

APPENDIX A: MEASURING THE COMPLETENESS FUNCTION

We have employed two methods to investigate how the mean subhalo count is affected by the finite resolution of an *N*-body simulation. In the following, we give a more detailed description of the two methods, focusing on the advantages and limitations of each.

A1 Method A: comparing low- and high-resolution simulations

The simplest way to investigate numerical effects is to compare the subhalo population of haloes of a given mass simulated at two different resolutions. For this, we use the two MS that resolve haloes of similar mass with 125 times better resolution in MS-II than in MS. Same mass haloes have, on average, $\overline{N}_{\rm MS}(\nu)$ and $\overline{N}_{\text{MS-II}}(\nu)$ substructures in MS and MS-II, respectively. According to equation (5), the ratio of the two subhalo numbers is given by

$$\frac{\overline{N}_{\rm MS}(\nu)}{\overline{N}_{\text{MS-II}}(\nu)} = \frac{f_{\rm MS}(\nu)}{f_{\text{MS-II}}(\nu)}, \tag{A1}$$

where $f_{\rm MS}(\nu)$ and $f_{\text{MS-II}}(\nu)$ are the completeness functions for the two MS. Because of the higher resolution of MS-II, we can recover the full subhalo population down to lower ν values than in MS. Thus, this expression can be rewritten as

$$f_{\rm MS}(\nu) = \frac{\overline{N}_{\rm MS}(\nu)}{\overline{N}_{\text{MS-II}}(\nu)}, \quad \text{as long as } f_{\text{MS-II}}(\nu) \cong 1. \tag{A2}$$

This holds down to the lowest value of ν for which MS-II resolves all substructures.

Fig. A1 shows the ratio between the subhalo number counts in the MS and MS-II simulations, for two samples of haloes in the mass range $(0.69\text{–}1.1) \times 10^{13}\, h^{-1}\,{\rm M}_\odot$ and $(0.6\text{–}1.2) \times 10^{14}\, h^{-1}\,{\rm M}_\odot$. The lower mass haloes are resolved in MS with $\sim 10^4$ particles while the higher mass ones are resolved with $\sim 10^5$ particles. We can see that resolution effects become important at $\nu \approx 0.6$ and $\nu \approx 0.3$ for haloes resolved with 10^4 and 10^5 particles. By increasing the number of particles by a factor of 10, we would resolve the subhaloes down to approximately two times lower values of ν. Since MS-II has 125 times higher resolution than MS, it recovers all the subhaloes down to $\sim$4 times lower ν than MS, which, according to the figure,

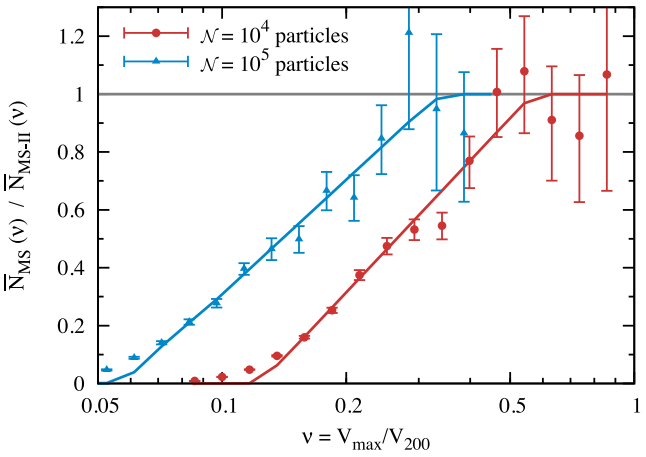

Figure A1. Method A for computing the completeness function. This method compares the subhalo number count, $\overline{N}(\nu)$, in haloes of a given mass resolved at two different resolutions in MS and MS-II. The two data sets consist of host haloes in the mass range $(0.69–1.1) \times 10^{13}\, h^{-1}\, M_\odot$ (red filled circles) and $(0.6–1.2) \times 10^{14}\, h^{-1}\, M_\odot$ (blue filled triangles). These are resolved in MS with $(0.8–1.2) \times 10^4$ and $(0.7–1.3) \times 10^5$ particles, respectively. The same haloes are resolved in MS-II with 125 times more particles. The two solid lines represent the completeness function fit given by equation (6). The error bars represent the 1σ uncertainty in the determination of the $\overline{N}_{MS}(\nu)/\overline{N}_{MS\text{-}II}(\nu)$ ratio.

corresponds to $\overline{N}_{MS}(\nu)/\overline{N}_{MS\text{-}II}(\nu) \sim 0.1$. This means that we can use equation (A2) to compute $f_{MS}(\nu)$ as long as $f_{MS}(\nu) \gtrsim 0.1$.

We find that the completeness function given by equation (6) gives a very good fit to the $\overline{N}_{MS}(\nu)/\overline{N}_{MS\text{-}II}(\nu)$ ratio. This is illustrated by the solid lines in Fig. A1 for haloes resolved with 10^4 and 10^5 particles. The fit is a good match to the completeness function for ν values for which $f(\nu) \geq 0.2$. At lower ν values, the completeness function has a more complex behaviour that is not captured by the two parameter expression that we use. Therefore, we limit our analysis and fits to regions with $f(\nu) \geq 0.2$.

Method A for estimating the completeness function is very simple and straightforward but its simplicity hides a major obvious disadvantage: it requires a second simulation with ∼100 times higher mass resolution than the original. To overcome this limitation, we introduce a different method for computing the completeness function which relies on a single simulation. We use method A to show that this method B gives the same results.

A2 Method B: comparing LM and HM haloes in the same simulation

In a cosmological simulation, subhaloes are resolved to lower values of ν in larger haloes. Thus, if we assume that the true number of subhaloes as function of ν, $\widetilde{N}(\nu)$ (see equation 5), is self-similar amongst host haloes of different mass (see Fig. 9 and Wang12), then we can derive the completeness function by comparing the substructure ν function in LM versus HM haloes.

To illustrate this method, we consider two halo samples: an LM and a HM sample. Furthermore, we choose the HM haloes to be Θ times more massive than their LM counterparts. In the limit when $\widetilde{N}(\nu)$ is independent of host halo mass,[3] the ratio between the number of substructure in the LM and HM samples is given by

$$\frac{\overline{N}_{LM}(\nu)}{\overline{N}_{HM}(\nu)} = \frac{f_{LM}(\nu)}{f_{HM}(\nu)}, \tag{A3}$$

where $f_{LM}(\nu)$ and $f_{HM}(\nu)$ are the completeness functions of the two halo samples. Using the $f(\nu)$ expression from equation (6), the above relation becomes

$$\begin{cases} 1 & \nu_0^{LM} \leq \nu \\ 1 + \alpha^{LM} \ln\left(\frac{\nu}{\nu_0^{LM}}\right) & \nu_0^{HM} \leq \nu < \nu_0^{LM} \\ \frac{1+\alpha^{LM} \ln\left(\frac{\nu}{\nu_0^{LM}}\right)}{1+\alpha^{HM} \ln\left(\frac{\nu}{\nu_0^{HM}}\right)} & \nu_0^{LM} e^{-1/\alpha^{LM}} \leq \nu < \nu_0^{HM} \\ 0 & \nu < \nu_0^{LM} e^{-1/\alpha^{LM}}, \end{cases} \tag{A4}$$

where $(\nu_0^{LM}, \alpha^{LM})$ and $(\nu_0^{HM}, \alpha^{HM})$ are the completeness function fit parameters corresponding to the LM and HM halo samples, respectively. This expression can be simplified further given that haloes in the two samples are resolved with $\mathcal{N}^{LM}$ and $\mathcal{N}^{HM} = \Theta\mathcal{N}^{LM}$ particles. This, combined with the dependence of the fit parameters, $\nu_0 \propto \mathcal{N}^{n_\nu}$ and $\alpha \propto \mathcal{N}^{n_\alpha}$, found in Section 3.1, results in

$$\nu_0^{HM} = \nu_0^{LM} \Theta^{n_\nu} \quad \text{and} \quad \alpha^{HM} = \alpha^{LM} \Theta^{n_\alpha}. \tag{A5}$$

Using these expressions reduces equation (A4) to 4 parameters: ν_0^{LM}, α^{LM}, n_ν and n_α. These fit parameters can be found using the following algorithm.

(i) Select a value for the mass ratio, $\Theta \sim$ a few.[4]
(ii) Make an initial guess for the parameters n_ν and n_α.
(iii) Select as the LM sample all haloes in a chosen mass range. The HM sample then contains all haloes Θ times more massive than this. Using these two samples find the best-fitting values of the parameters ν_0^{LM} and α^{LM}.
(iv) Repeat the previous step for different host halo masses in order to obtain the parameters ν_0^{LM} and α^{LM} for a wide range of halo masses.
(v) Use the dependence on mass, and therefore on host particle number, $\mathcal{N}$, of ν_0^{LM} and α^{LM} found in the previous step to find new values for n_ν and n_α.
(vi) Check if n_ν and n_α have converged to the values used as the input for step (iii). If the values have converged, stop the iterative procedure. Otherwise, repeat steps (iii) through (vi) using the latest values for n_ν and n_α.

In Fig. A2, we illustrate the use of method B to compute the completeness function for the three N-body simulations used in this study. The figure shows the ratio, $\overline{N}_{LM}(\nu)/\overline{N}_{HM}(\nu)$, of the mean number of subhaloes in the LM and HM halo samples. We plot this ratio for LM haloes resolved with $\sim 10^4$, $\sim 10^5$ and $\sim 10^6$ particles, with masses given in Table A1. To minimize the variation of the subhalo number counts with mass, we take the HM sample to be $\Theta = 3$ times more massive than the LM one. The fit given by equation (A4) is shown as a solid curve for each of the data sets. We can see that it gives a very good fit for $\overline{N}_{LM}(\nu)/\overline{N}_{HM}(\nu) \geq 0.4$,

[3] In reality, $\widetilde{N}(\nu)$ varies slowly with host mass. To mitigate this effect, we only compare halo samples that differ in mass only by a factor, $\Theta \sim$ a few.

[4] We have checked that the mass ratio, Θ, of the LM and HM samples does not affect the fit parameters. While we recommend using $\Theta = 3$, we have checked that similar fit parameters are obtained for $2 \leq \Theta \leq 10$. Using larger values of Θ introduces artefacts because of the mass dependence of $\overline{N}(\nu)$, while using smaller values results in very noisy fit parameters.

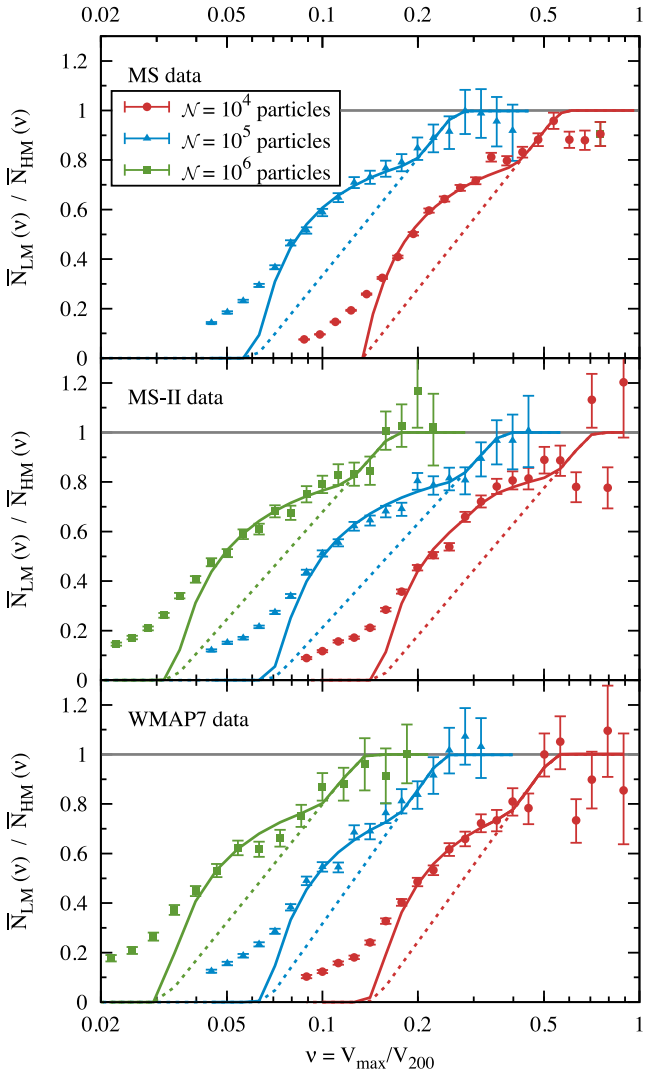

Figure A2. Method B for computing the completeness function for the MS (top panel), MS-II (centre panel) and *WMAP*7 (bottom panel) simulations. The method uses the ratio of the subhalo abundance, $\overline{N}(\nu)$, between LM and HM halo samples. The red, blue and green lines and symbols correspond to LM haloes resolved with (0.8–1.2) $\times$ 10^4, (0.8–1.2) $\times$ 10^5 and (0.8–1.2) $\times$ 10^6 particles in each of the three simulations. The halo mass ranges used for each data set are given in Table A1. The solid curves represent the fit given by equation (A4) to each data set. The dashed lines show the inferred completeness function, $f_{LM}(\nu)$, for the LM sample. The error bars represent the 1σ uncertainty in the determination of the $\overline{N}_{LM}(\nu)/\overline{N}_{HM}(\nu)$ ratio.

Table A1. The mass range of haloes resolved with $\mathcal{N} = (0.8–1.2) \times 10^4$, $\mathcal{N} = (0.8–1.2) \times 10^5$ and $\mathcal{N} = (0.8–1.2) \times 10^6$ particles in the MS, MS-II and *WMAP*7 simulations. These halo samples were used to obtain the results presented in Fig. A2. We only give the mass range for the LM halo sample, since haloes in the HM sample are always $\Theta = 3$ times more massive than these.

Simulation	$\mathcal{N} \sim 10^4$	$\mathcal{N} \sim 10^5$	$\mathcal{N} \sim 10^6$
MS	(0.68–1.03) $\times$ $10^{13}\,h^{-1}\,M_\odot$	(0.68–1.03) $\times$ $10^{14}\,h^{-1}\,M_\odot$	–
MS-II	(5.5–8.3) $\times$ $10^{10}\,h^{-1}\,M_\odot$	(5.5–8.3) $\times$ $10^{11}\,h^{-1}\,M_\odot$	(5.5–8.3) $\times$ $10^{12}\,h^{-1}\,M_\odot$
*WMAP*7	(5.0–7.5) $\times$ $10^{10}\,h^{-1}\,M_\odot$	(5.0–7.5) $\times$ $10^{11}\,h^{-1}\,M_\odot$	(5.0–7.5) $\times$ $10^{12}\,h^{-1}\,M_\odot$

which corresponds to values $f_{LM}(\nu) \geq 0.2$, the same limit for which Method A is also accurate.

Fig. A2 shows another important result. The completeness function has the same parametric form, given by equation (6), for all the three simulations used in this study. This is a reflection of the fact that equation (A4) gives a very good fit to the $\overline{N}_{LM}(\nu)/\overline{N}_{HM}(\nu)$ ratio for the three simulations: MS, MS-II and *WMAP*7.

Computing the completeness function using method B has the advantage of not requiring a simulation with a higher mass resolution as in method A. This opens up the possibility of quantifying how numerical effects in any given simulation alter the mean subhalo abundance. We illustrated this for MS-II and *WMAP*7 for which we do not have a higher resolution version and so we cannot apply method A. The main limitation of method B stems from the assumption that the mean subhalo abundance is self-similar amongst host haloes of different mass. As we found in Section 5, this condition is satisfied for substructures in DM-only simulations, but it will not be the case when adding in baryons. The complex feedback processes involved in galaxy formation affect haloes of different mass in different ways (e.g. Sawala et al. 2013, and references within). This breaks the self-similar behaviour of the subhalo abundance.

APPENDIX B: COMPARISON OF ROCKSTAR AND SUBFIND SUBHALO ABUNDANCES

Here, we investigate if the difference in the subhalo numbers between our analysis and previous studies can be explained by the use of different halo finders. For this, we compare the galactic subhalo abundance as found by ROCKSTAR (Behroozi et al. 2013) and by SUBFIND (Springel et al. 2001), with the latter used in the studies of Wang12 and BK10.

We apply the same analysis steps to SUBFIND subhaloes as we did in the case of ROCKSTAR: identify the number of missing substructures due to resolution effects and estimate the true subhalo abundance, following the procedure described in Section 3. The resulting subhalo abundance for MW-mass hosts is well described by equation (9) with best-fitting parameters: $a = -3.18$, $\nu_1 = 0.333$, $b = 6$ and $\nu_{cut} = 0.78$ (for subhaloes found within a distance R_{200} from the host). Fig. B1 compares the subhalo abundance found with ROCKSTAR and SUBFIND, showing that for $\nu \lesssim 0.3$ both halo finders get the

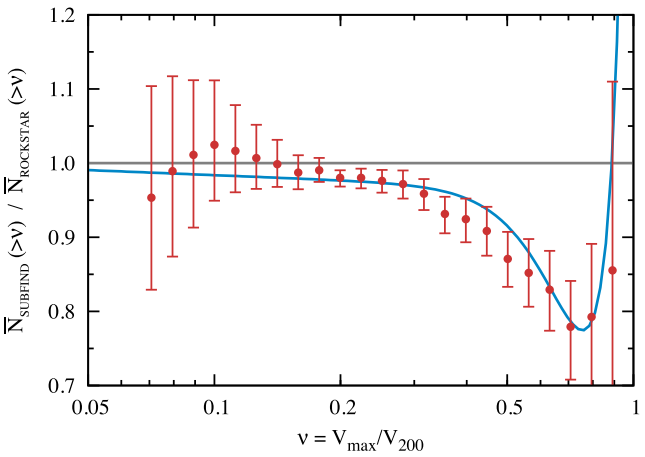

Figure B1. Comparison of the subhalo abundance of galactic mass haloes identified with SUBFIND versus that found with ROCKSTAR. The points give the $\overline{N}_{SUBFIND}(>\nu)/\overline{N}_{ROCKSTAR}(>\nu)$ ratio as measured in the MS-II. The solid curve shows the ratio between the best-fitting function (see equation 9) to the SUBFIND and ROCKSTAR subhalo abundance.

same number of substructures, up to a few per cent difference. For higher ν, SUBFIND identifies $\sim$10 per cent fewer substructures. Given that such massive subhaloes are resolved with $\gtrsim 10^3$ particles, the difference is likely due to substructures found close to the centre of the host that are identified by ROCKSTAR, which is a phase-space halo finder, and not by SUBFIND, which uses only real-space information. Since Wang12 computed the subhalo abundance only in the interval $0.1 \leq \nu \leq 0.5$, the figure clearly shows that the use of ROCKSTAR instead of SUBFIND cannot on its own explain the $\sim$20 per cent higher subhalo abundance found in our study. Similarly, the significantly lower value of the subhalo abundance slope, a, found by BK10 is not due to the use of a different halo finder.

This paper has been typeset from a TEX/LATEX file prepared by the author.